

The Fractal Distribution of HII Regions in Disk Galaxies

Néstor Sánchez¹ and Emilio J. Alfaro¹

nestor@iaa.es

ABSTRACT

It is known that the gas has a fractal structure in a wide range of spatial scales with a fractal dimension that seems to be a constant around $D_f \simeq 2.7$. It is expected that stars forming from this fractal medium exhibit similar fractal patterns. Here we address this issue by quantifying the degree to which star-forming events are clumped. We develop, test, and apply a precise and accurate technique to calculate the correlation dimension D_c of the distribution of HII regions in a sample of disk galaxies. We find that the determination of D_c is limited by the number of HII regions, since if there are $\lesssim 100$ regions available then a bias tending to underestimate the dimension is produced. The reliable results are distributed in the range $1.5 \lesssim D_c \lesssim 2.0$ with an average value $\langle D_c \rangle = 1.81$. This corresponds to a three-dimensional dimension of $\langle D_f \rangle = 2.73$, very similar to the value measured in the interstellar clouds. However, we get significant variations in the fractal dimension among galaxies, contrary to a universal picture sometimes claimed in literature. The fractal dimension exhibits a weak but significant correlation with the absolute magnitude and, to a lesser extent, with the galactic radius. The faintest galaxies tend to distribute their HII regions in more clustered (less uniform) patterns. The fractal dimension for the brightest HII regions within the same galaxy seems to be smaller than for the faintest ones suggesting some kind of evolutionary effect, but the obtained correlation remains unchanged if only the brightest regions are taken into account.

Subject headings: HII regions — catalogs — galaxies: structure — stars: formation

1. Introduction

One important issue in Astronomy is how the structure and distribution of interstellar gas at different spatial scales is connected to the distribution of newborn stars in the

¹Instituto de Astrofísica de Andalucía, CSIC, Apdo. 3004, E-18080, Granada, Spain.

host galaxy. It is known that the gas follows a hierarchical and self-similar structure in a wide range of scales from ~ 0.1 pc to ~ 1 kpc (Elmegreen & Scalo 2004; Bergin & Tafalla 2007). The fractal dimension characterizing this self-similar structure seems to have a nearly universal value around $D_f \simeq 2.7$ (Sánchez et al. 2005, 2007b). This value is in perfect agreement with recent simulations of compressively driven turbulence in the Interstellar Medium done by Federrath et al. (2007), who obtained $D_f \simeq 2.6 - 2.7$ in their standard simulations. In principle one would expect that newborn stars forming from the high density peaks in these fractal regions should exhibit similar fractal patterns (Elmegreen & Elmegreen 2001). The analysis of the young stellar population belonging to the Gould Belt yielded a fractal dimension $D_f = 2.68 \pm 0.04$ that is consistent with this picture (Sánchez et al. 2007a). However, late-type stars in the Gould Belt have a significantly larger fractal dimension ($D_f = 2.85 \pm 0.04$). There exist several possible causes for this difference (see the discussion in Sánchez et al. 2007a) but one possibility is that these two stellar populations simply are reflecting two different gas distributions of the parental clouds at different spatial scales according to a multifractal scenario (Chappell & Scalo 2001; de la Fuente Marcos & de la Fuente Marcos 2006).

To test this possibility detailed studies of fractal properties at larger spatial scales are required. There is clear evidence that gas also follows fractal patterns at galactic scales (i.e. larger than the kpc). For example, the HI distribution displays a scale-free nature in SMC (Stanimirovic et al. 1999), LMC (Kim et al. 2003), and other external galaxies (both irregulars and spirals) with very different intrinsic properties (Westpfahl et al. 1999; Willett et al. 2005; Begun et al. 2006; Dutta et al. 2008). A fractal (or multifractal) topology can explain some galactic properties such as flat rotation curves (Pfenniger & Combes 1994) or the Kennicutt-Schmidt star formation law (Tassis 2007). What about the spatial distribution of newborn stars at galactic scales? Again, a hierarchical and self-similar picture is consistent with the distribution of star fields and star-forming sites on galaxy-wide scales (Feitzinger & Galinski 1987; Elmegreen & Elmegreen 2001; Elmegreen et al. 2003; Parodi & Binggeli 2003; Elmegreen et al. 2006; de la Fuente Marcos & de la Fuente Marcos 2006; Odekon 2006; Bastian et al. 2007). However, it is not clear whether this kind of fractal distributions are connected/related or not to some properties of the host galaxies, such as radius, rotation, brightness, morphology, etc. In spite of the great variety of D_f values reported in the literature for different galaxies (for both the gas and the distribution of star forming sites) most of the authors argue in favor of a more or less universal picture (see the references already mentioned). In this universal description, the constancy of the fractal dimension is a natural consequence of the fact that the same physical processes are structuring these systems. However, there are some indications that the situation could be different and the mechanism that arrange the gas at spatial scales larger than ~ 1 kpc could modify the

final distribution of the star formation at such scales. The fractal dimension of the distribution of HII regions could be different in grand design and flocculent galaxies (as suggested by Hodge 1985), and the brightest galaxies could have fractal dimensions higher than faintest ones (Parodi & Binggeli 2003; Odekon 2006). On the contrary, Feitzinger & Galinski (1987) do not find any correlation between the fractal dimension and the galactic properties, but their uncertainties are so large that the robustness of this conclusion is questionable.

Part of the problem that prevents achieving unequivocal conclusions lies in the great diversity of analysis techniques used in the literature and/or the application to not large enough samples of galaxies. This paper aims to contribute to fill this gap by providing, firstly, a carefully designed method that has been tested on simulated data and that clearly establishes its accuracy and applicability depending on the sample itself. Therefore, this method can be used in a reliable way to investigate the distribution of HII regions in disk galaxies. We apply this method to the most complete sample of galaxies that we have found in literature expecting to draw significant conclusions regarding this matter. This paper is organized as follows. Section 2 explains the method used to calculate the fractal dimension. It also analyzes the problems arising from projection and sample size effects. Section 3 describes the data collected from different sources on which we apply the method in Section 4. The possible correlations between the fractal dimension of the distribution of HII regions and other galactic properties are discussed in Section 5. Finally, the main results are summarized in Section 6.

2. The fractal dimension of disk-like point distributions

The primary goal of this work is to calculate the fractal dimension of the distribution of HII regions in galaxies. One way to do this is by using the so-called correlation dimension (Grassberger & Procaccia 1983) which gives robust results when dealing with distributions of points in space. Let us consider N points in space with positions \mathbf{x} . The number of other points within a sphere of radius r centered on the i -th point is given by

$$n_i(r) = \sum_{j=1, j \neq i}^N H(r - |\mathbf{x}_i - \mathbf{x}_j|) \quad , \quad (1)$$

where $H(x)$ is the Heaviside step function. We can choose M different points as centers and then calculate the commonly called correlation integral in the form

$$a(r) = \frac{1}{M(N-1)} \sum_{i=1}^M n_i(r) \quad . \quad (2)$$

Thus, this quantity represents the probability of finding a point within a sphere of radius r centered on another point. For a fractal set $C(r)$ scales at small r as

$$C(r) \sim r^{D_c} \quad , \quad (3)$$

being D_c the correlation dimension. For a homogeneous distribution of points in a plane we expect $D_c = 2$, whereas if the points are distributed obeying a fractal geometry then $D_c < 2$. When evaluating $C(r)$ for real data the power-law behavior (eq. 3) is valid only within a limited range of r values, even if the distribution follows an underlying fractal law. If r is of the order of the mean distance between nearest neighbors then the distribution looks like a set of isolated points. Furthermore, if r tends to the full data set size then boundary effects become increasingly important. In both cases $C(r)$ deviates from the expected power-law behavior and D_c tends to be underestimated (see Sánchez et al. 2007a, and references mentioned therein). These effects are magnified when the number of available data decrease. We have developed an algorithm to calculate D_c in a reliable way for two-dimensional distributions of points (Sánchez et al. 2007a). The novelty of the algorithm lies in the implementation of objective and suitable criteria to avoid both boundary effects and finite-data problems at small scales. First, the algorithm finds the boundary of the set of points by using the procedure proposed by Eddy (1977), which determines the vertices of the minimum-area convex polygon containing the whole set of data points. Then we place circles of different radii and evaluate $C(r)$ according to equations (1) and (2). For this we impose the condition that all circles must be kept inside the sample, this means that circles are not allowed to cross the previously defined boundary. The calculation is done for r values ranging from the minimal distance between two points to the maximum allowable value. The number of possible samplings M decreases as r increases. In each case we calculate both $C(r)$ and the corresponding standard deviation σ_C . The correlation dimension D_c is given by the slope of the best linear fit in a $\log C - \log r$ plot. We establish a lower limit for this fit given by the r value for which $\sigma_C = C(r)$. This simple criterion removes poorly estimated $C(r)$ values occurring mainly at small r values. An upper limit is automatically set by the largest circle fitting into the sample. Finally, the uncertainty associated to D_c is calculated using bootstrap techniques: we repeat the calculation on a series of random resamplings of the data and the standard deviation of the obtained set of D_c values is taken as the error in our estimation (σ_{boot}). This algorithm yields very good results for distributions of points with a well-defined fractal dimension D_f (monofractals). For simulated two-dimensional fractals with $1 < D_f < 2$ we verified that the relation $D_c - \sigma_{boot} \lesssim D_f \lesssim D_c + \sigma_{boot}$ is always fulfilled (Sánchez et al. 2007a). That is, the algorithm gives unbiased fractal dimensions for sufficiently representative samples.

What we observe on the image of an external galaxy is the distribution of HII regions projected onto the celestial sphere. From the inclination and position angles we can obtain

the image as projected on the mean plane of the galaxy. One important question is the relationship between the correlation dimension measured on this plane (let us call it D_c) and the “real” dimension of the three-dimensional distribution of HII regions within the volume occupied by the galactic disk (D_f). On the one hand, if the total thickness of the galactic disk Z_{disk} is much more smaller than the galactic diameter D_{gal} , i.e. if $f \equiv Z_{disk}/D_{gal} \ll 1$, then the system can be considered as a very thin slice of the three-dimensional distribution. In this case, the dimension of the three-dimensional distribution and the two-dimensional dimension are related through the expression (Falconer 1990)

$$D_c = D_f - 1 \quad . \quad (4)$$

On the other hand, if we have the extreme case $f \simeq 1$, then the image should be treated as a projection of the three-dimensional set and the expected result is (Falconer 1990)

$$D_c = \min\{2, D_f\} \quad . \quad (5)$$

In a previous paper (Sánchez et al. 2005) we showed that for real fractals¹ the dimension measured on the projected image tends to be lower than the theoretical value given by eq. (5).

2.1. Projection effects

In a disk galaxy the value of f for the distribution of HII regions would be some intermediate value between a perfect slice ($f = 0$) and a projection ($f = 1$). For a typical galaxy like the Milky Way this value should be around $f \sim 100 \text{ pc}/10 \text{ kpc} = 0.01$ (e.g. Paladini et al. 2004). In order to assess how the slice thickness f would alter the results we have done some numerical tests. First, we have generated three-dimensional fractals following a simple recipe in order to ensure a perfectly defined fractal dimension. Within a cube of size R (half of cube height) we placed 8 smaller cubes (one in each octant) with size R/L ($L \geq 2$). Each cube is placed randomly but always within the volume of its corresponding octant. This procedure is repeated successively H times such as at the end we get a distribution of 8^H points (we have used $H = 8$ which yields ~ 16 millions of points). The fractal dimension of this distribution is given by $D_f = \log 8 / \log L$. For the extreme case $L = 2$ we get a homogeneous distribution with $D_f = 3$, but if $L > 2$ then $D_f < 3$. Then we took a slice along a random plane in space and projected it onto its mean plane. The ratio f between the slice thickness and the size of the fractal is set by hand and is kept as a free parameter.

¹By “real” fractals we mean distributions of points following an underlying fractal law but not infinite in spatial scale or in number of points and, moreover, having some random component.

Finally, we randomly removed points from the fractal until reaching the desired sample size N which was also kept as a free parameter.

What we have done is to study in detail how the calculated dimension D_c depends on the original dimension D_f . Figure 1 shows the results for three different values of f but the same sample size ($N = 1000$ points). The error bars in this figure come from the random component in the fractal generation process. In general, these error bars tend to be higher at low D_f values because as D_f decreases the filling factor decreases and, therefore, the random component increases when each child cube is placed. In other words, these error bars are related to the random variations when generating the fractals and not to the uncertainties in the determination of D_c (σ_{boot}), the latter ones always being smaller than the former ones. The result for the case $f = 1$ is quite similar to the previously reported (Sánchez et al. 2005): the projected dimension tends to be smaller than the theoretical value given by equation (5). This is because the projection on random planes may produce random groupings and this implies a decrease in D_c . This behavior is less pronounced or even non-existent for the cases $D_f \simeq 3$ (the projection of a homogeneous distribution of points is again homogeneous) and $D_f \simeq 1$ (the probability of occurrence of chance groupings is low because the filling factor is also low). In general, the projection on the mean plane does not affect the results for the very thin slice case ($f = 10^{-4}$) with the calculated values being very close to the theoretical values expected for a zero-thickness slice (eq. 4). The random fluctuations involved in the simulations tend to “hide” the fractal structure, randomizing any underlying fractal pattern. This may yield D_c values slightly higher than expected for a perfect slice. An interesting point is that when D_f decreases too much, structures belonging to lower levels of the hierarchy are so small in comparison with the slice thickness that the resulting distribution is essentially equivalent to a projection on the mean plane of the slice. This change in behavior from thin slice to projection can be clearly seen in Figure 1. The slice-projection transition zone depends, obviously, on both D_f and f : as the slice thickness increases the projection behavior appears at higher D_f values. In any case, we have obtained a nearly linear $D_c - D_f$ relationship when $D_c \gtrsim 1.5$. Moreover, this relationship is almost independent of the exact f value as long as it is around or less than the typical value $f \simeq 0.01$ (compare, for example, cases $f = 10^{-2}$ and $f = 10^{-4}$ in Figure 1). Thus, any uncertainty in f would translate into a large uncertainty when estimating D_f from D_c only if $D_c \ll 1.5$ and/or $f \gg 10^{-2}$. Otherwise the fractal dimension would be well-determined. We will see later that our “reliable” results for the distribution of HII regions in galaxies lie in the range $1.5 \leq D_c \leq 2.0$. Table 1 presents the resulting values for $D_c \geq 1.5$. The results shown correspond to the case $f = 10^{-2}$ but, as mentioned before, these results do not significantly depend on the exact f value.

2.2. Sampling size effects

How does the measured dimension depend on the sample size? This is an important question because when working with observational data many times the number of available data points is rather small. There can be both extrinsic causes for this (biased subsamples due to selection effects or criteria in the detection of HII regions) and intrinsic ones (for example, very low star formation rates would produce a small number of clearly distinguishable HII regions). Previously (Sánchez et al. 2007a) we showed that D_c tended to be underestimated in two-dimensional fractals having a relatively small number of points. This effect could yield unrealistic results and/or trends. In order to quantify this effect we repeated the previous calculations with the same fractals and slices but randomly removing more points until reaching smaller sample sizes N . Figure 2 shows the results for $f = 10^{-4}$ and two different fractal dimensions $D_f = 3$ and $D_f = 2$, for which the expected values for thin slices are $D_c = 2$ and $D_c = 1$, respectively (indicated by horizontal lines). Since we are dealing exactly with the same original data, the observed decreasing in the average D_c value with decreasing N have to be attributed exclusively to sample size itself. Thus, in general, the algorithm is able to estimate the fractal dimension in a reliable way when applied to random subsamples of fractal distributions of points. However, if the sample size is too small ($N \lesssim 100$) a bias tending to underestimate the dimension is produced.

3. The sample of galaxies

We have used VizieR² (Ochsenbein et al. 2000) and ADS³ databases, in conjunction with the papers of Garcia-Gomez & Athanassoula (1991) and Garcia-Gomez et al. (2002), to search for catalogs of external galaxies containing positions of HII regions available in machine readable format. We found a total of 93 spiral galaxies with positions for at least 50 HII regions. If several different catalogs were available for the same galaxy we choose the one having the largest amount of data. We have also included data for 8 irregular galaxies with HII positions kindly provided by D. Hunter (Roye & Hunter 2000). The properties of the selected galaxies are listed in Table 2. The columns contain the following information: (1) galaxy name, (2) morphological Hubble type, (3) and (4) position ϕ and inclination i angles respectively (in degrees), (5) morphological type encoded in the de Vaucouleurs scale T , (6) spiral arm class A , (7) distance to the galaxy D (in Mpc), (8) B-band absolute magnitude M_B , (9) radius corresponding to the isophotal level 25 mag/arcsec² in the B-band R_{25} (in

²<http://vizier.u-strasbg.fr>

³<http://adswwww.harvard.edu>

kpc), (10) maximum rotation velocity corrected for inclination V_{rot} (in km s^{-1}), and (11) the reference from which positions of HII regions were obtained (Ref). Most of the data for spiral galaxies was taken from HyperLeda⁴ database (Paturel et al. 2003). The arm class was taken from Elmegreen & Elmegreen (1987). The position and inclination angles were taken from Garcia-Gomez & Athanassoula (1991) and Garcia-Gomez et al. (2002), if available, or from HyperLeda otherwise. All the data for irregular galaxies come from Roye & Hunter (2000). Figure 3 shows the deprojected distributions of HII regions for each galaxy considered here according to the references given in the last column of Table 2.

4. The fractal dimension of the HII region distributions

It can be the case that clustering properties of HII regions differ from region to region in the same galaxy. These differences may be due to some bias (as, for example, if a smaller amount of data exists in a more poorly observed region of the galaxy) or they may be real differences (for example, the organizing role of spiral waves will be smaller close to the central region). Obviously, the algorithm returns only an average estimation of D_c for the entire distribution of points. Given the sufficiently representative sample of galaxies we expect that this effect does not affect our main results and conclusions. One important point that has to be taken into consideration while estimating D_c is the possible presence of outliers. If a relatively small number of points are clearly separated from the rest of the data then the resulting D_c value could be artificially low because of the presence of large empty spaces. The algorithm takes this possibility into account in a first approximation by defining the boundary. The points that determine the boundary are not considered in the calculation because any circle including any of these points is automatically outside the boundary. Thus, it does not matter if any of these points is an outlier because it is not used in the calculation. However, we have added an additional criterion to minimize possible problems arising from this effect: if a small fraction of points (we have chosen 10% of the total sample) is located outside R_{25} then those points are removed from the calculation. This criterion does not affect the results if those points are not actually outliers. The points that have been excluded from the calculation are surrounded by circles in Figure 3.

The result of calculating the correlation dimension of the distribution of HII regions in the sample of galaxies is shown in Table 3. The columns are the galaxy name, the number of cataloged HII regions N , the calculated dimension D_c , the uncertainty resulting from bootstrapping σ_{boot} , and the range of spatial scales $R_{min} - R_{max}$ (in kpc) over which the HII

⁴<http://leda.univ-lyon1.fr>

regions are distributed. The calculated D_c values are also shown in parenthesis in Figure 3. It can be seen that D_c is consistent with the appearance of the HII region distributions. D_c values close to 2 correspond to nearly homogeneous distributions. Smaller D_c values correspond to more irregular distributions having clumps and/or filaments separated by low density (or empty) regions. As an example, we can compare the smallest and the largest D_c values in first page of Figure 3: NGC 337A ($D_c = 1.34$) exhibits a much more clumpy distribution than the relatively homogeneous galaxy NGC 1068 ($D_c = 1.99$).

Figure 4 shows the calculated correlation dimension for all the galaxies in the sample as a function of the number of available data points. The first thing we note is that there exist significant differences among the galaxies: in general, the uncertainties in the determination of the dimension (σ_{boot}) are smaller than the dispersion of the obtained values ($\sigma \simeq 0.3$). This result differs considerably from the conclusion outlined by Feitzinger & Galinski (1987) for their sample of 19 spiral galaxies who argued in favor of a constant D_c around the mean value $\langle D_c \rangle = 1.68$. Two trends are clearly visible in Figure 4. First, the uncertainties increase as $N(\text{HII})$ decreases, consistent with the results obtained in the previous simulations. But moreover, at small number of regions the obtained values are substantially more spread out toward lower values. The results were averaged in bins of the number of HII regions with each bin having approximately the same number of galaxies (~ 25). Table 4 summarizes the results, where for each bin we show mean values (also shown in Figure 4), medians, and standard deviations both for the fractal dimensions and for the corresponding uncertainties. The overall trend, i.e. the convergence of the mean value to a certain value (in this case ~ 1.8) as the number of data points increases, is very similar to the behavior described for the simulated fractals (Figure 2). It is clear that at least part of this trend is due to a bias in the estimated value of D_c for galaxies with small number of HII regions. It is only when $N(\text{HII}) \gtrsim 200$ that we obtain uncertainties below $\sigma_{boot} = 0.1$. Therefore, to overcome this bias, we focus the detailed analysis (next section) on galaxies having more than 200 HII regions (46 spiral galaxies). The average fractal dimension in this case is $\langle D_c \rangle = 1.81$ with a standard deviations of $\sigma = 0.14$. According to the results of Section 2 (Table 1) this corresponds to an average three-dimensional dimension of $\langle D_f \rangle = 2.73$. Our average result is very similar (within the uncertainties) to the result of Feitzinger & Galinski (1987) ($\langle D_c \rangle = 1.68$). However, the average uncertainty obtained by Feitzinger & Galinski (1987) is ~ 0.3 whereas we get an average σ_{boot} of ~ 0.03 . By considering these associated uncertainties we can say that, contrary to our results, their D_c values do not differ among themselves. Regarding the irregular galaxies, we have only a very small number of galaxies (8) and they have no more than 200 HII regions (the value we are considering as the limit for an unbiased determination of D_c). Thus, any conclusion based on these data should be treated with great caution. The average fractal dimension for irregulars is $\langle D_c \rangle = 1.79$

(similar to that found for spirals) with a standard deviation of $\sigma = 0.20$. The average value for σ_{boot} is 0.14 so that there are not significant variations among these galaxies. The results obtained by Parodi & Binggeli (2003) are spread over the range $1.2 \lesssim D_c \lesssim 2.0$, but if we only consider their five galaxies having ~ 200 or more HII regions then this range narrows to $1.55 \lesssim D_c \lesssim 1.62$. This is below our average result mostly because our result represents a lower limit in the case of bias due to small sample size.

5. Dependence on galactic properties

At this point, we have a set of fractal dimension values determined in a precise and accurate way and a set of variables describing some galactic properties, such as the position angle ϕ , inclination i , morphological type T , arm class A , distance D , absolute magnitude M_B , radius of the isophotal 25 R_{25} , rotation velocity V_{rot} , and the number of HII regions $N(\text{HII})$. Now we proceed to examine possible correlations between the fractal dimension and these variables but taken into account that they represent properties of different nature. Some of these quantities are in some way involved in the determination of the fractal dimension and may, therefore, introduce some bias or uncertainties into the calculated D_c values. These biases can be introduced either by taking part directly in the calculation or through the observation or deprojection processes. If this is the case then spurious correlations can arise. We refer to these as *intrinsic* properties; they are ϕ , i , D , and $N(\text{HII})$. On the other hand, the rest of the observed variables are related to galactic properties but they do not participate directly in the determination of D_c ; these *extrinsic* variables are T , A , M_B , R_{25} , and V_{rot} . We also analyze a new variable that we have called the average surface density of star forming regions, given by the number of star forming regions divided by the square of the radius ($N(\text{HII})/R_{25}^2$).

5.1. Analysis method

The main goal is to identify possible relationships between the degree of clumpiness of HII regions in galaxies and their *intrinsic* and/or *extrinsic* properties, in the above sense. So we have to suggest a model of dependence and evaluate its “goodness” via some statistical test defined for such purpose. We propose, in a first approximation, a linear model linking the variables and we choose as statistical criterion the *AIC* (Akaike’s Information Criterion, Akaike 1974), defined as $AIC = 2k - 2 \ln(L)$ where L is the maximized likelihood value and k is the number of estimable parameters in the model. Let RSS be the residual sum of squares and n the number of observations, then the *AIC* becomes $AIC = 2k + n [\ln(2\pi RSS/n) + 1]$.

Increasing the number of free parameters to be estimated improves the goodness of fit, regardless of the number of free parameters in the data generating process. Hence *AIC* not only rewards goodness of fit, but also includes a penalty that is an increasing function of the number of estimated parameters. This penalty discourages overfitting. The preferred model is the one with the lowest *AIC* value. Once the best model has been selected according to this criterion we perform the *t* and *F* tests to infer the significance of the coefficients of the model and of the overall fit. This analysis is performed in the **R** environment for statistical computing (R Development Core Team 2008).

5.2. Intrinsic variables

We begin with the intrinsic variables (ϕ , i , D , and $N(\text{HII})$) and considering first the whole sample of galaxies. Starting from a linear regression model based on n variables we apply a stepwise regression process to select the subset of variables providing the best model. The analysis yields the position angle of the major axis and the number of HII regions as the most significant variables. Thus, the best model to explain D_c variations from these variables has the form $D_c = a\phi + bN(\text{HII}) + c$. However, both the *t*-test for the regression coefficients and the *F*-test for the overall fit indicate no significance at 95% confidence level. This result supports our previous finding in simulated fractal distributions: the number of HII regions in a galaxy affects the quality of the estimated fractal dimension by introducing a systematic bias and a noise. The presence of the variable $N(\text{HII})$ in the model is simply the result of the existence of this bias. If we exclude those objects with $N(\text{HII}) < 200$ and repeat the analysis, we obtain that any variable is able to significantly explain the observed variance in the fractal dimension.

5.3. Extrinsic variables

Now we will consider the variables T , A , M_B , R_{25} , V_{rot} , and $N(\text{HII})/R_{25}^2$, and we will restrict the analysis to galaxies having $N(\text{HII}) > 200$. Figure 5 shows D_c as a function of each one of these variables. First we construct an initial linear model incorporating all of these variables. The application of the task *step* (within the package *stats* of **R**) yields that the variables M_B and R_{25} represent the best liner model fitting the data, this is

$$D_c = -(0.069 \pm 0.025)M_B - (0.006 \pm 0.003)R_{25} + 0.456 \quad . \quad (6)$$

The overall fit gives $F = 4.0$ that for degrees of freedom 2 and 43 is significant at the confidence level of 95%. The regression coefficients of the variables M_B and R_{25} are significant

at the confidence levels of 99% and 95% (marginally significant), respectively.

According to our results D_c correlates with M_B and, to a lesser extent, with R_{25} . Brightest galaxies have fractal dimensions higher than faintest ones (Figure 5c). A slight trend is apparent in Figure 5c in which the correlation with M_B appears to saturate for galaxies brighter than $M_B \simeq -21$, but the large scatter in this M_B interval prevents us from drawing a general conclusion. Feitzinger & Galinski (1987) find a pure scatter diagram when comparing D_c and M_B which, together with the lack of correlation with other properties is used as argument favoring a universal D_c value in spiral galaxies. The dependence on M_B that we observe is probably hidden by their imprecise determination of D_c (uncertainties of the order of ~ 0.3). In contrast, Parodi & Binggeli (2003) report the same trend in their sample of dwarf irregulars, i.e. the highest fractal dimensions for the brightest galaxies. They applied a correction factor to the calculated D_c to take account of differences in the number of HII regions. However, their results have to be taken with caution because, as mentioned before, it is a little disturbing that they have only five galaxies with $N(\text{HII}) \gtrsim 200$ for which the correlation does not exist at all. Odekon (2006) analyzed in detail the distribution of resolved young stars in star-forming dwarf galaxies. Unfortunately she used only four galaxies, but she obtained that the brightest galaxy had the highest fractal dimension and the faintest galaxy the lowest. The interpretation given by Parodi & Binggeli (2003) is that a small D_c value implies a higher intragalactic gas porosity which reduces the (massive) star formation rate (Silk 1997). The same argument remains valid for spiral galaxies if the presence of density waves does not greatly affect the star formation process (Elmegreen & Elmegreen 1986). For the irregular galaxies in our sample, we find that the average fractal dimension ($\simeq 1.79$) is similar within the uncertainties to that found for spirals with $N(\text{HII}) \gtrsim 200$ ($\simeq 1.81$). Moreover, it is higher than that for spirals with $N(\text{HII}) < 200$ ($\simeq 1.65$) although, statistically, there is no significative difference. Curiosity prompted us to check what happens when irregular galaxies are included in the previous statistical analyses, and what we find is that the correlation disappears. Dwarf irregular galaxies are characterized by fractal dimensions similar to those of the brightest spiral galaxies, so that any possible correlation between D_c and M_B is removed when both types of galaxies are considered. Even if we try to correct the small sample size bias in the irregulars, the resulting D_c values would be higher and this effect would be enhanced. Therefore, in spite of the small number of irregular galaxies studied, we can conclude that if D_c is a function of M_B in irregulars (as suggested by Parodi & Binggeli 2003) this correlation does not follow the same law as for spirals; and the fractal dimension for irregulars is, on average, higher than for spirals with the same absolute magnitude.

5.4. Possible evolutionary effects

If we assume that star formation takes place mainly along the spiral arms then the inter-arm regions should typically exhibit older HII regions. This kind of evolutionary effect have been proposed to explain variations in the luminosity functions of HII regions in the spiral arms versus the inter-arm regions (e.g. Oey & Clarke 1998). We wonder whether this kind of effect could introduce some bias because in principle one would expect that only the brightest regions are visible for the farthest (and faintest) galaxies. However, we didn't detect any correlation between the calculated D_c value and the galaxy's distance so that our results would seem to be unaffected by this possible effect. In any case, we have analyzed the dependence of D_c on the brightness of the HII regions for those galaxies with enough available data. We first selected galaxies from the sample for which we have data on HII region brightness and a sample size large enough ($N(\text{HII}) > 600$) to calculate D_c in a reliable way for the brightest 1/3 of the HII regions. There are a total of 9 galaxies fulfilling these requirements: NGC 628, NGC 3344, NGC 3486, NGC 3631, NGC 3726, NGC 4254, NGC 4303, NGC 4321, and NGC 6946 (the reference for this data is Bradley et al. 2006). We divided the sample in three equal subsamples ordered in descending brightness: the brightest HII regions (high-brightness), the medium bright ones (medium-brightness), and the faintest ones (low-brightness). Figure 6 shows, as an illustrative example, the resulting distributions in NGC 6946 for which we have little more than ~ 500 HII regions in each case. We recalculated D_c for each case and the results are shown in Table 5. The general trend is that D_c is smaller for the brightest HII regions than for the rest of the data. This can be seen by eye from inspection of Figure 6 where the left-side panel exhibits, clearly, a more clumpy morphology. The only exceptions to this general trend are NGC 4254 that exhibits the opposite behavior and NGC 4303 that does not show any significant variation. The rest of the galaxies have a smaller D_c value for the brightest HII regions. These regions should reflect, in a first approximation, the initial distribution of star-forming regions in each galaxy. It seems likely from our results that some kind of evolutionary effect tends to randomize (homogenize) in some degree the initial distributions of HII regions.

Does this result affect the correlations we found in the previous sections? We have repeated the analysis replacing the full sample D_c values by the high-brightness values for the 9 galaxies in Table 5. First we use all the galaxies having more than 200 HII regions (46 galaxies). In this case, the analysis yields exactly the same variables for the best fit (eq. 6) with nearly the same F value (4.1) and a confidence level of 99% for the overall fit. The coefficients for M_B and R_{25} are -0.069 and -0.007 with confidence levels of 99% and 95%, respectively. We have also tested what happens if we take only the galaxies having more than 200 and less than 600 HII regions and the high-brightness values for the 9 galaxies in Table 5. The idea behind this selection criterion is to avoid galaxies having a “mixed”

(bright and faint) population of HII regions. Again, the analysis yields M_B and R_{25} as the variables providing the best fit to the data. The fit gives $F = 4.6$ that for degrees of freedom 2 and 37 is significant at the 95%. The coefficients obtained in this case for M_B and R_{25} are -0.079 and -0.006 with confidence levels of 99% and 90%, respectively. Summarizing, when only the bright HII regions are considered the trend shown in eq. (6) is preserved, i.e. the correlation strength with M_B remains the same (or even increases) whereas the correlation with R_{25} is, in the best scenario, marginally significant.

6. Conclusions

The study of the distribution of HII regions in galaxies may provide important clues to understanding the processes involved in the star formation at galactic scales. Our approach in this work has been apply a precise and accurate technique to calculate the degree of self-similar clumpiness (the correlation dimension D_c) in a large enough sample of disk galaxies. All the obtained dimensions are shown in Table 3. Our most reliable results are distributed in the range $1.5 \lesssim D_c \lesssim 2.0$ with an average value $\langle D_c \rangle = 1.81$. This value corresponds to a three-dimensional dimension of $\langle D_f \rangle = 2.73$. The similarity between this value and the value $D_f \simeq 2.7 \pm 0.1$ measured in interstellar molecular clouds (Sánchez et al. 2007b) may seem, in principle, unexpected given the very different spatial scales involved. There are many energy sources that can drive the turbulence and structure the interstellar medium (Elmegreen & Scalo 2004), but this structure can be modified at a galactic level due to the action of other physical processes acting at this larger spatial scales. The fractal behavior we have observed span a range of scales from ~ 10 pc to ~ 25 kpc, and we have not found any dependence on the spatial scales involved.

The uncertainties of the most reliable D_c values are small enough (~ 0.03 on average) to allow us to conclude that there are significant variations among galaxies. This conclusion is incompatible with a universal picture in which the fractal dimension is approximately a constant for the spiral galaxies (Feitzinger & Galinski 1987). We have found that D_c exhibits a weak but significant correlation with M_B and, to a lesser extent, with R_{25} . The faintest galaxies tend to distribute the HII regions in a more clumpy or clustered way. It is the first time that this behavior is reported in spiral galaxies, but it is in agreement with similar results suggested for irregular galaxies (Parodi & Binggeli 2003; Odekon 2006). Moreover, the fractal dimension for the brightest HII regions tends to be smaller than for the faintest ones. This behavior could be the result of some kind of evolutionary effect that tends to randomize in some degree the initial distribution of HII regions (Oey & Clarke 1998). However, if only the brightest HII regions are taken into account the observed correlation

with M_B and R_{25} remains unchanged. We have not found correlations with other galactic properties (morphological type, spiral arm class, rotation velocity, and surface density of HII regions). There are many galactic properties from which D_c could depend, such as star formation activity, mass, age, metallicity, or a combination of them. It has been suggested that the fractal dimension of the distribution of star-forming sites could be increased during the star formation process (for example, de la Fuente Marcos & de la Fuente Marcos 2006, and this work). A more complete analysis including more galactic variables and a wider and more diverse sample of galaxies would be necessary in order to obtain a clearer picture.

We acknowledge D. Hunter for providing the data on irregular galaxies. We also thank an anonymous referee for his/her comments, which improved this paper and led us to add Section 5.4 to an earlier version of this paper. This research has made use of NASA's Astrophysics Data System and of HyperLeda and VizieR databases. We acknowledge financial support from MEC of Spain through grant AYA2007-64052 and from Consejería de Educación y Ciencia (Junta de Andalucía) through TIC-101.

REFERENCES

- Akaike, H. 1974, IEEE Transactions on Automatic Control, 19, 716
- Bastian, N., Ercolano, B., Gieles, M., Rosolowsky, E., Scheepmaker, R. A., Gutermuth, R., & Efremov, Y. 2007, MNRAS, 379, 1302
- Begun, A., Chengalur, J. N., & Bhardwaj, S. 2006, MNRAS, 372, L33
- Bergin, E. A. & Tafalla, M. 2007, ARA&A45, 339
- Bradley, T. R., Knapen, J. H., Beckman, J. E., & Folkes S. L. 2006, A&A, 459, L13
- Chappell, D. & Scalo, J. 2001, ApJ, 551, 712
- Courtes, G., Petit, H., Hua, C. T., Martin, P., Blecha, A., Huguenin, D., & Golay, M. 1993, A&A, 268, 419
- de la Fuente Marcos, R., & de la Fuente Marcos, C. 2006, MNRAS, 372, 279
- Dutta, P., Begum, A., Bharadwaj, S., & Chengalur, J. N. 2008, MNRAS, 384, L34
- Eddy, W. F. 1977, *Trans. Math. Soft.*, 3, 398
- Elmegreen, D. M. & Elmegreen, B. G. 1987, ApJ, 314, 3

- Elmegreen, B. G., & Elmegreen, D. M. 1986, *ApJ*, 311, 554
- Elmegreen, B. G. & Elmegreen, D. M. 2001, *AJ*, 121, 1507
- Elmegreen, B. G., Elmegreen, D. M., Chandar, R., Whitmore, B., & Regan, M. 2006, *ApJ*, 644, 879
- Elmegreen, B. G., Elmegreen, D. M., & Leitner, S. N. 2003, *ApJ*, 590, 271
- Elmegreen, B. G. & Scalo, J. 2004, *ARA&A*42, 211
- Evans, I. N., Koratkar, A. P., Storchi-Bergmann, T., Kirkpatrick, H., Heckman, T. M., & Wilson A. S. 1996, *ApJS*, 105, 93
- Falconer, K. J. 1990, *Fractal Geometry: Mathematical Foundations and Applications* (London: Wiley)
- Federrath, C., Schmidt, W., & Klessen, R. S. 2007, preprint (arXiv:0710.1359)
- Feinstein, C. 1997, *ApJS*, 112, 29
- Feitzinger, J. V., & Galinski, T. 1987, *A&A*, 179, 249
- Garcia-Gomez, C., & Athanassoula, E. 1991, *A&AS*, 89, 159
- Garcia-Gomez, C., Athanassoula, E., & Barbera, C. 2002, *A&A*, 389, 68
- Gonzalez-Delgado, R. M., Perez, E., Tadhunter, C., Vilchez, J. M., & Rodriguez-Espinosa, J. M. 1997, *ApJS*, 108, 155
- Grassberger, P., & Procaccia, I. 1983, *Phys. Rev. Lett.*, 50, 346
- Hodge, P. 1985, *PASP*, 97, 688
- Hodge, P., Gurwell, M., Goldader J. D., & Kennicutt, R. C. Jr. 1990, *ApJS*, 73, 661
- Hodge, P. W., Balsley, J., Wyder, T. K., & Skelton, B. P. 1999, *PASP*, 111, 685
- Kim, S., Staveley-Smith, L., Dopita, M. A., Sault, R. J., Freeman, K. C., Lee, Y., & Chu, Y.-H. 2003, *ApJS*, 148, 473
- Knapen, J. H., Arnth-Jensen, N., Cepa, J., & Beckman, J. E. 1993, *AJ*, 106, 56
- Lin, W., Zhou, X., Burstein, D., Windhorst, R. A., Chen, J., Chen, W.-P., Jiang, Z., Kong, X., Ma, J., Sun, W.-H., Wu H., Xue, S., & Zhu J. 2003, *AJ*, 126, 1286

- Ochsenbein, F., Bauer, P., Marcout, J. 2000, *A&AS*, 143, 221
- Odekon, M. C. 2006, *AJ*, 132, 1834
- Oey, M. S. & Clarke, C. J. 1998, *AJ*, 115, 1543
- Paladini, R., Davies, R. D., & DeZotti, G. 2004, *MNRAS*, 347, 237
- Parodi, B. R., & Binggeli, B. 2003, *A&A*, 398, 501
- Paturel, G., Petit, C., Prugniel, Ph., Theureau, G., Rousseau, J., Brouty, M., Dubois, P., & Cambresy, L. 2003, *A&A*, 412, 45
- Pellet, A., Astier, N., Viale, A., Courtes, G., Maucherat, A., Monnet, G., & Simien, F. 1978, *A&AS*, 31, 439
- Petit, H., Hua, C. T., Bersier, D., & Courtes G. 1996, *A&A*, 309, 446
- Petit, H. 1998, *A&AS*, 131, 317
- Pfenniger, D., & Combes, F. 1994, *A&A*, 285, 94
- R Development Core Team 2008, *R: A Language and Environment for Statistical Computing*, R Foundation for Statistical Computing, Vienna, Austria, URL <http://www.R-project.org>, ISBN 3-900051-07-0
- Roye, E. W., & Hunter, D. A. 2000, *AJ*, 119, 1145
- Rozas, M., Zurita, A., Heller, C. H., & Beckman, J. E. 1999, *A&AS*, 135, 145
- Rozas, M., Zurita, A., & Beckman, J. E. 2000, *A&A*, 354, 823
- Silk, J. 1997, *ApJ*, 481, 703
- Sánchez, N., Alfaro, E. J., & Pérez, E. 2005, *ApJ*, 625, 849
- Sánchez, N., Alfaro, E. J., Elias, F., Delgado, A. J., & Cabrera-Caño, J. 2007a, *ApJ*, 667, 213
- Sánchez, N., Alfaro, E. J., & Pérez, E. 2007b, *ApJ*, 656, 222
- Stanimirovic, S., Staveley-Smith, L., Dickey, J. M., Sault, R. J., & Snowden, S. L. 1999, *MNRAS*, 302, 417
- Tassis, K. 2007, *MNRAS*, 382, 1317

Tsvetanov, Z. I., & Petrosian A. R. 1995, ApJS, 101, 287

Westpfahl, D. J., Coleman, P. H., Alexander, J., & Tongue, T. 1999, AJ, 117, 868

Willett, K. W., Elmegreen, B. G., & Hunter, D. A. 2005, AJ, 129, 2186

Table 1. Results for the simulated fractals for the $f = 10^{-2}$ case (see text)

D_f	D_c	$\sigma_{boot,ave}$ ¹
2.40	1.47	0.02
2.45	1.52	0.02
2.50	1.57	0.02
2.55	1.63	0.02
2.60	1.68	0.02
2.65	1.73	0.02
2.70	1.78	0.02
2.75	1.83	0.02
2.80	1.88	0.02
2.85	1.92	0.02
2.90	1.96	0.02
2.95	1.98	0.02
3.00	2.00	0.02

¹Average of the calculated uncertainties, as determined from bootstrapping

Table 2. Properties of the galaxies in the sample

Name	type	ϕ	i	T	A	D	M_B	R_{25}	V_{rot}	Ref.
Spirals										
ESO 377-24	Sc	100	35	5.0	...	39.5	-20.10	8.14	129.9	(1)
IC 2510	SBb	152	60	2.5	...	37.5	...	8.68	133.7	(1)
IC 2560	SBb	42	57	3.3	...	39.2	-21.16	20.15	195.9	(1)
IC 3639	SBbc	105	20	4.1	...	44.9	-20.48	8.21	215.1	(1)
NGC 210	SABb	162	57	3.1	6	22.0	-20.41	15.89	154.3	(2)
NGC 224	Sb	38	77	3.0	...	1.0	-21.71	25.53	249.8	(3)
NGC 337A	SABd	8	56	7.9	2	14.2	-18.65	5.45	39.3	(2)
NGC 598	Sc	23	55	6.0	5	1.1	-19.38	9.62	100.4	(4)
NGC 628	Sc	23	8	5.2	9	9.8	-20.61	14.02	38.0	(2)
NGC 864	SABc	24	48	5.1	5	9.8	-20.57	14.02	133.0	(2)
NGC 1042	SABc	6	16	6.0	9	21.8	-20.23	11.82	144.7	(2)
NGC 1068	Sb	84	29	3.0	3	18.0	-21.38	10.16	320.9	(2)
NGC 1073	SBc	163	30	5.3	5	15.3	-19.91	13.55	38.6	(2)
NGC 1097	SBb	130	50	3.3	12	16.4	-21.22	8.43	299.3	(5)
NGC 1300	Sbc	101	49	4.0	12	15.2	-20.93	23.51	167.1	(2)
NGC 1566	SABb	41	32	4.0	12	20.2	-21.43	18.18	104.0	(1)
NGC 1672	Sb	170	34	3.3	5	17.4	-20.74	18.08	201.7	(5)
NGC 1808	Sa	128	48	1.2	...	15.0	-19.90	13.62	122.9	(1)
NGC 2775	Sab	160	41	1.7	3	10.9	-20.60	8.62	291.4	(2)
NGC 2805	SABc	116	39	6.9	5	19.2	-20.84	11.88	70.7	(2)
NGC 2985	Sab	180	36	2.3	3	28.1	-20.81	13.87	225.4	(2)
NGC 2997	SABc	100	40	5.1	9	22.6	-21.39	11.89	222.1	(6)
NGC 3031	Sab	150	58	2.4	12	13.1	-21.54	19.48	223.8	(7)
NGC 3081	S0-a	91	39	0.0	6	5.3	-19.99	16.53	99.9	(1)
NGC 3169	Sa	45	57	1.1	2	31.8	-20.34	12.21	321.0	(8)
NGC 3184	SABc	90	13	5.9	9	17.7	-19.88	11.14	125.3	(2)
NGC 3227	SABa	157	68	1.4	7	10.9	-20.12	11.77	130.0	(2)
NGC 3344	Sbc	164	28	4.0	9	17.5	-19.66	10.14	209.9	(2)

Table 2—Continued

Name	type	ϕ	i	T	A	D	M_B	R_{25}	V_{rot}	Ref.
NGC 3351	Sb	13	39	3.0	6	9.9	-20.23	9.57	176.7	(2)
NGC 3359	Sc	171	52	5.2	5	11.8	-20.53	12.35	148.6	(9)
NGC 3367	Sc	100	40	5.2	9	18.0	-21.39	10.68	172.8	(8)
NGC 3368	SABa	5	55	1.8	8	44.3	-20.90	18.02	194.0	(2)
NGC 3393	SBa	80	27	1.1	...	13.4	-20.83	16.48	168.8	(1)
NGC 3486	Sc	80	42	5.2	9	51.7	-19.61	14.46	125.4	(2)
NGC 3631	Sc	150	22	5.2	9	11.6	-21.00	9.84	78.4	(2)
NGC 3660	Sbc	120	37	3.9	2	19.9	-21.16	10.74	230.7	(8)
NGC 3726	Sc	14	49	5.1	5	52.0	-20.63	19.36	159.0	(2)
NGC 3783	SBa	137	30	1.3	9	15.4	-21.09	11.78	126.7	(1)
NGC 3810	Sc	32	48	5.2	2	38.9	-20.12	12.31	152.1	(2)
NGC 3982	SABb	7	21	3.2	2	15.2	-19.83	7.35	190.4	(8)
NGC 4030	Sbc	19	40	4.0	9	19.8	-20.76	5.30	229.4	(2)
NGC 4051	SABb	132	40	4.0	5	21.1	-19.96	11.60	213.1	(2)
NGC 4123	Sc	141	42	5.0	9	13.1	-19.84	9.31	128.5	(2)
NGC 4151	SABa	50	21	2.1	5	19.5	-20.05	9.04	144.3	(2)
NGC 4254	Sc	61	30	5.2	9	16.9	-22.59	7.08	193.5	(2)
NGC 4258	SABb	157	72	4.0	...	35.8	-21.04	26.21	208.0	(10)
NGC 4303	Sbc	135	29	4.0	9	9.7	-21.82	25.88	213.8	(2)
NGC 4321	SABb	153	32	4.0	12	23.1	-22.06	23.13	225.0	(2)
NGC 4395	Sm	127	18	8.8	1	2.7	-17.29	1.66	50.3	(2)
NGC 4487	Sc	74	46	5.9	5	14.7	-19.56	7.38	119.7	(2)
NGC 4507	Sab	60	33	1.9	5	47.7	-20.92	9.57	...	(1)
NGC 4535	Sc	181	44	5.0	9	29.0	-21.95	34.41	176.6	(2)
NGC 4548	Sb	150	37	3.1	5	8.5	-20.81	6.83	163.2	(2)
NGC 4579	SABb	89	39	2.8	9	22.9	-21.68	16.71	263.1	(2)
NGC 4593	Sb	80	44	3.0	5	35.3	-20.81	12.33	295.8	(1)
NGC 4602	SABb	96	65	4.3	...	36.4	-20.75	6.82	207.0	(1)
NGC 4618	SBm	40	58	8.6	4	10.7	-19.29	5.51	65.6	(2)
NGC 4639	Sbc	127	55	3.5	2	15.4	-19.15	6.44	163.5	(5)
NGC 4689	Sc	163	31	4.7	3	24.6	-20.69	13.66	135.1	(2)

Table 2—Continued

Name	type	ϕ	i	T	A	D	M_B	R_{25}	V_{rot}	Ref.
NGC 4699	SABb	47	47	3.0	3	19.9	-21.49	13.76	256.9	(8)
NGC 4725	SABa	32	54	2.1	6	19.5	-21.77	27.50	225.4	(2)
NGC 4736	Sab	118	37	2.4	3	7.5	-20.81	8.49	166.9	(2)
NGC 4939	Sbc	19	56	4.0	12	44.3	-22.16	36.82	220.1	(1)
NGC 4995	SABb	100	50	3.1	6	25.0	-20.58	8.81	163.2	(8)
NGC 5033	Sc	171	62	5.2	9	15.4	-20.87	22.10	223.3	(5)
NGC 5194	Sbc	170	20	4.0	12	10.0	-20.51	11.25	140.2	(11)
NGC 5247	SABb	170	38	4.1	9	18.9	-21.16	14.59	95.6	(2)
NGC 5248	SABb	146	61	4.0	12	17.8	-20.86	10.57	144.8	(2)
NGC 5334	Sc	18	45	5.1	2	20.5	-19.13	10.07	133.7	(2)
NGC 5364	Sbc	37	52	4.0	9	18.9	-20.88	10.44	170.1	(6)
NGC 5371	Sbc	7	39	4.0	9	39.8	-22.12	23.03	222.5	(2)
NGC 5427	SABc	90	30	5.0	9	39.4	-21.23	20.68	376.9	(1)
NGC 5457	SABc	39	18	5.9	9	7.2	-21.03	25.00	202.4	(12)
NGC 5474	Sc	85	50	6.0	2	7.4	-16.06	2.58	22.6	(2)
NGC 5643	Sc	70	30	4.9	...	14.8	-20.90	11.34	168.7	(1)
NGC 5681	Sb	152	56	3.5	...	114.9	-21.39	14.49	187.9	(6)
NGC 5850	Sb	108	47	3.1	8	37.7	-21.48	18.35	117.4	(2)
NGC 5921	Sbc	149	36	4.0	8	22.6	-20.55	9.92	95.2	(2)
NGC 5964	SBcd	147	42	6.9	2	22.2	-18.89	11.05	120.8	(2)
NGC 6070	Sc	65	60	6.0	9	30.0	-21.09	15.21	201.4	(6)
NGC 6118	Sc	57	70	5.9	...	23.5	-20.80	15.20	163.1	(6)
NGC 6140	Sc	76	32	5.6	2	17.1	-19.15	5.21	169.3	(2)
NGC 6221	Sc	25	45	4.9	...	18.4	-21.63	12.90	162.9	(1)
NGC 6300	SBb	108	52	3.1	6	12.8	-20.30	10.32	173.2	(5)
NGC 6384	SABb	40	47	3.6	9	25.5	-21.48	9.11	182.5	(6)
NGC 6814	SABb	176	22	4.0	9	22.6	-21.42	10.16	31.8	(13)
NGC 6946	SABc	64	34	5.9	9	6.7	-20.89	11.07	190.9	(2)
NGC 7314	SABb	178	64	4.0	2	18.8	-20.48	11.49	150.5	(5)
NGC 7331	Sbc	170	77	3.9	3	14.1	-21.58	18.85	246.1	(14)
NGC 7479	SBbc	22	51	4.4	9	34.9	-21.70	18.47	273.0	(15)

Table 2—Continued

Name	type	ϕ	i	T	A	D	M_B	R_{25}	V_{rot}	Ref.
NGC 7552	Sab	181	37	2.4	...	20.2	-20.45	11.38	208.1	(6)
NGC 7590	Sbc	25	65	4.1	...	19.8	-20.08	8.78	182.5	(1)
NGC 7741	SBC	162	43	6.0	5	12.4	-19.30	6.53	105.7	(2)
Irregulars										
DDO 47	IB	100.0	66.0	9.8	...	2.8	-14.15	1.25	62	(16)
DDO 50	I	25.0	50.2	9.8	...	3.2	-16.93	3.70	41	(16)
DDO 154	I	49.5	59.5	9.9	...	4.0	-14.52	1.75	48	(16)
DDO 168	I	149.0	66.0	9.9	...	3.5	-15.43	1.85	55	(16)
IC 10	IB	137.5	54.5	9.9	...	1.0	-16.31	0.90	32	(16)
NGC 1156	IB	37.0	34.8	9.8	...	7.0	-18.00	3.75	60	(16)
NGC 2366	IB	34.5	71.2	9.8	...	3.2	-16.69	2.44	47	(16)
NGC 4214	I	33.0	22.7	9.8	...	4.8	-18.58	5.95	50	(16)

References. — (1) Tsvetanov & Petrosian (1995); (2) Bradley et al. (2006); (3) Pellet et al. (1978); (4) Hodge et al. (1999); (5) Evans et al. (1996); (6) Feinstein (1997); (7) Lin et al. (2003); (8) Gonzalez-Delgado et al. (1997); (9) Rozas et al. (2000); (10) Courtes et al. (1993); (11) Petit et al. (1996); (12) Hodge et al. (1990); (13) Knapen et al. (1993); (14) Petit (1998); (15) Rozas et al. (1999); (16) Roye & Hunter (2000).

Table 3. Calculated fractal dimensions

Name	N	D_c	σ_{boot}	$R_{min} - R_{max}$	Name	N	D_c	σ_{boot}	$R_{min} - R_{max}$
Spirals									
ESO 377-24	59	1.92	0.42	0.20 - 2.82	IC 2510	70	1.86	0.22	0.23 - 2.51
IC 2560	137	1.74	0.09	0.35 - 10.14	IC 3639	112	2.11	0.09	0.11 - 3.99
NGC 210	162	1.52	0.08	0.16 - 11.93	NGC 224	981	1.51	0.02	0.01 - 17.38
NGC 337A	189	1.34	0.05	0.05 - 9.93	NGC 598	1272	1.83	0.02	0.01 - 5.71
NGC 628	2027	1.84	0.01	0.03 - 9.27	NGC 864	226	1.68	0.04	0.10 - 6.65
NGC 1042	158	1.60	0.08	0.11 - 5.35	NGC 1068	166	1.99	0.07	0.09 - 5.65
NGC 1073	170	1.41	0.07	0.02 - 7.93	NGC 1097	402	1.78	0.03	0.01 - 16.30
NGC 1300	84	1.08	0.24	0.15 - 8.75	NGC 1566	679	1.77	0.02	0.04 - 9.79
NGC 1672	260	1.91	0.05	0.01 - 11.16	NGC 1808	206	1.70	0.06	0.04 - 2.36
NGC 2775	66	1.27	0.28	0.16 - 3.79	NGC 2805	94	1.60	0.11	0.15 - 12.05
NGC 2985	338	1.87	0.03	0.09 - 8.42	NGC 2997	373	1.89	0.04	0.19 - 11.29
NGC 3031	493	1.74	0.04	0.04 - 9.73	NGC 3081	75	1.89	0.23	0.10 - 3.14
NGC 3169	67	1.35	0.26	0.14 - 3.63	NGC 3184	576	1.70	0.02	0.04 - 8.51
NGC 3227	185	1.86	0.07	0.12 - 5.46	NGC 3344	669	1.78	0.03	0.03 - 6.63
NGC 3351	55	0.98	0.14	0.20 - 4.77	NGC 3359	547	1.83	0.02	0.12 - 13.53
NGC 3367	79	1.74	0.19	0.13 - 6.91	NGC 3368	77	0.86	0.21	0.06 - 3.74
NGC 3393	80	1.28	0.34	0.18 - 7.25	NGC 3486	612	1.78	0.02	0.03 - 7.89
NGC 3631	801	1.97	0.01	0.02 - 12.96	NGC 3660	59	1.30	0.27	0.40 - 8.08
NGC 3726	614	1.80	0.03	0.05 - 8.94	NGC 3783	58	2.07	0.27	0.21 - 1.99
NGC 3810	400	2.00	0.03	0.06 - 5.88	NGC 3982	117	2.00	0.11	0.06 - 1.71
NGC 4030	276	2.01	0.03	0.07 - 7.08	NGC 4051	232	1.74	0.07	0.08 - 5.60
NGC 4123	247	1.66	0.04	0.06 - 9.90	NGC 4151	262	1.53	0.03	0.09 - 12.97
NGC 4254	626	1.86	0.02	0.09 - 18.10	NGC 4258	137	1.79	0.09	0.32 - 12.86
NGC 4303	873	1.83	0.02	0.06 - 16.71	NGC 4321	2601	1.94	0.01	0.05 - 19.34
NGC 4395	498	1.49	0.02	0.01 - 2.51	NGC 4487	146	1.78	0.05	0.11 - 6.30
NGC 4507	92	1.62	0.21	0.21 - 4.24	NGC 4535	518	1.71	0.02	0.09 - 21.16
NGC 4548	74	1.16	0.15	0.03 - 1.74	NGC 4579	121	1.38	0.09	0.06 - 6.67
NGC 4593	112	1.28	0.15	0.08 - 8.03	NGC 4602	218	2.07	0.05	0.24 - 8.29

Table 3—Continued

Name	N	D_c	σ_{boot}	$R_{min} - R_{max}$	Name	N	D_c	σ_{boot}	$R_{min} - R_{max}$
NGC 4618	290	1.76	0.05	0.06 - 3.70	NGC 4639	190	1.89	0.06	0.01 - 5.18
NGC 4689	160	2.00	0.06	0.13 - 5.53	NGC 4699	104	1.77	0.13	0.26 - 4.18
NGC 4725	134	1.20	0.19	0.06 - 6.89	NGC 4736	294	1.71	0.04	0.03 - 3.21
NGC 4939	250	1.86	0.04	0.24 - 19.39	NGC 4995	142	1.91	0.09	0.04 - 3.99
NGC 5033	423	2.00	0.03	0.31 - 15.89	NGC 5194	478	2.05	0.03	0.01 - 7.97
NGC 5247	157	1.61	0.07	0.09 - 7.79	NGC 5248	381	1.88	0.03	0.07 - 15.14
NGC 5334	106	1.57	0.18	0.10 - 5.76	NGC 5364	174	2.04	0.05	0.32 - 11.62
NGC 5371	264	1.66	0.06	0.16 - 14.01	NGC 5427	300	1.78	0.04	0.10 - 10.93
NGC 5457	1264	1.76	0.01	0.05 - 25.82	NGC 5474	165	1.46	0.06	0.04 - 3.34
NGC 5643	214	1.77	0.05	0.04 - 4.79	NGC 5681	55	2.06	0.38	2.55 - 22.09
NGC 5850	155	1.31	0.10	0.20 - 16.99	NGC 5921	274	1.77	0.04	0.08 - 12.77
NGC 5964	111	1.55	0.13	0.09 - 8.99	NGC 6070	62	2.00	0.31	0.69 - 6.98
NGC 6118	119	2.09	0.11	0.41 - 10.81	NGC 6140	127	1.58	0.07	0.08 - 7.79
NGC 6221	173	1.70	0.06	0.08 - 4.83	NGC 6300	317	1.97	0.05	0.01 - 7.45
NGC 6384	283	2.03	0.04	0.38 - 16.84	NGC 6814	734	1.87	0.02	0.07 - 8.05
NGC 6946	1528	1.75	0.01	0.02 - 8.00	NGC 7314	151	2.06	0.09	0.01 - 7.02
NGC 7331	252	1.90	0.05	0.09 - 15.51	NGC 7479	1009	1.70	0.02	0.08 - 18.07
NGC 7552	78	1.88	0.13	0.29 - 5.55	NGC 7590	129	2.01	0.10	0.07 - 3.30
NGC 7741	246	1.66	0.05	0.06 - 5.54					
Irregulars									
DDO 47	57	1.63	0.21	0.05 - 1.42	DDO 50	89	1.56	0.10	0.06 - 1.72
DDO 154	55	1.83	0.14	0.06 - 0.70	DDO 168	49	2.09	0.20	0.07 - 0.64
IC 10	79	1.64	0.14	0.03 - 0.48	NGC 1156	95	2.07	0.11	0.12 - 1.70
NGC 2366	97	1.75	0.18	0.06 - 2.22	NGC 4214	186	1.73	0.05	0.06 - 3.88

Table 4. Summary of calculated fractal dimensions

HII regions	D_c			σ_{boot}		
	mean	median	sta.dev.	mean	median	sta.dev.
$N < 100$	1.62	1.64	0.37	0.22	0.21	0.08
$100 < N < 175$	1.71	1.72	0.28	0.09	0.09	0.04
$175 < N < 375$	1.79	1.77	0.16	0.05	0.05	0.01
$375 < N$	1.81	1.80	0.13	0.02	0.02	0.01

Table 5. Fractal dimensions for different HII region brightness

Galaxy	High-brightness		Medium-brightness		Low-brightness	
	D_c	σ_{boot}	D_c	σ_{boot}	D_c	σ_{boot}
NGC 628	1.75	0.02	1.87	0.02	1.83	0.02
NGC 3344	1.76	0.04	1.87	0.05	1.89	0.05
NGC 3486	1.74	0.03	1.77	0.06	1.81	0.07
NGC 3631	1.84	0.04	1.90	0.05	1.94	0.04
NGC 3726	1.63	0.07	1.75	0.06	1.92	0.06
NGC 4254	1.88	0.05	1.79	0.06	1.70	0.06
NGC 4303	1.83	0.04	1.82	0.04	1.83	0.04
NGC 4321	1.79	0.02	1.89	0.02	1.83	0.02
NGC 6946	1.64	0.03	1.82	0.03	1.79	0.03

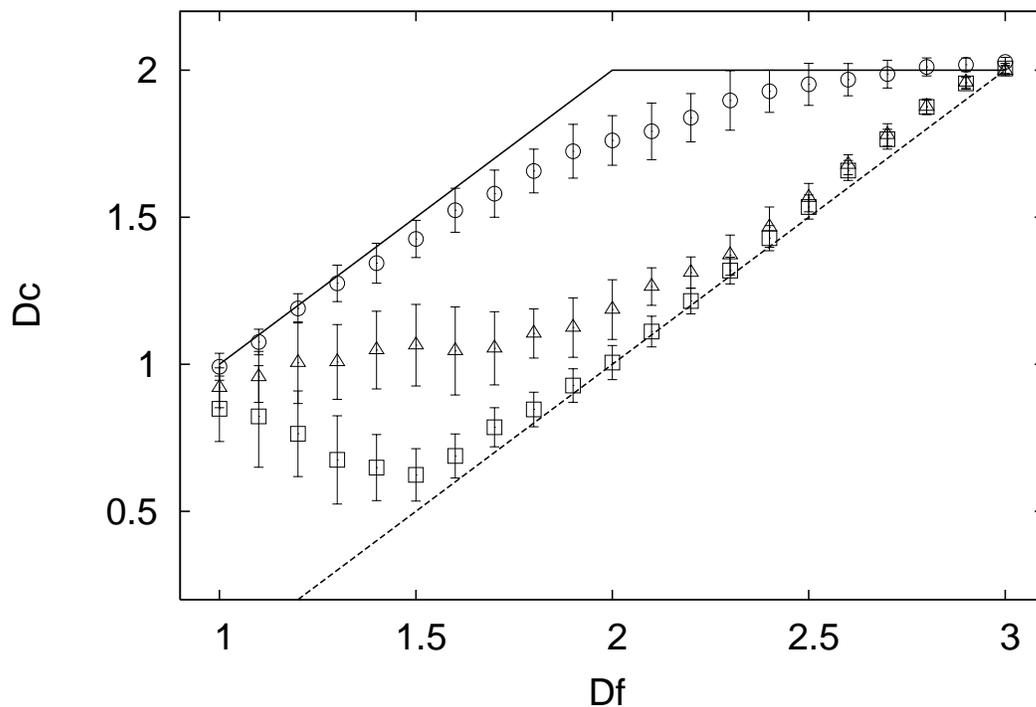


Fig. 1.— Calculated dimension D_c as a function of the fractal dimension D_f for three different values of the slice thickness: $f = 1$ (open circles), $f = 10^{-2}$ (open triangles), and $f = 10^{-4}$ (open squares). The number of points for the fractals is $N = 1000$. Each point is the result of calculating the average of 50 random fractals, and the bars indicate the standard deviations. The solid and dashed lines show the theoretical results for a projection and a thin slice, respectively.

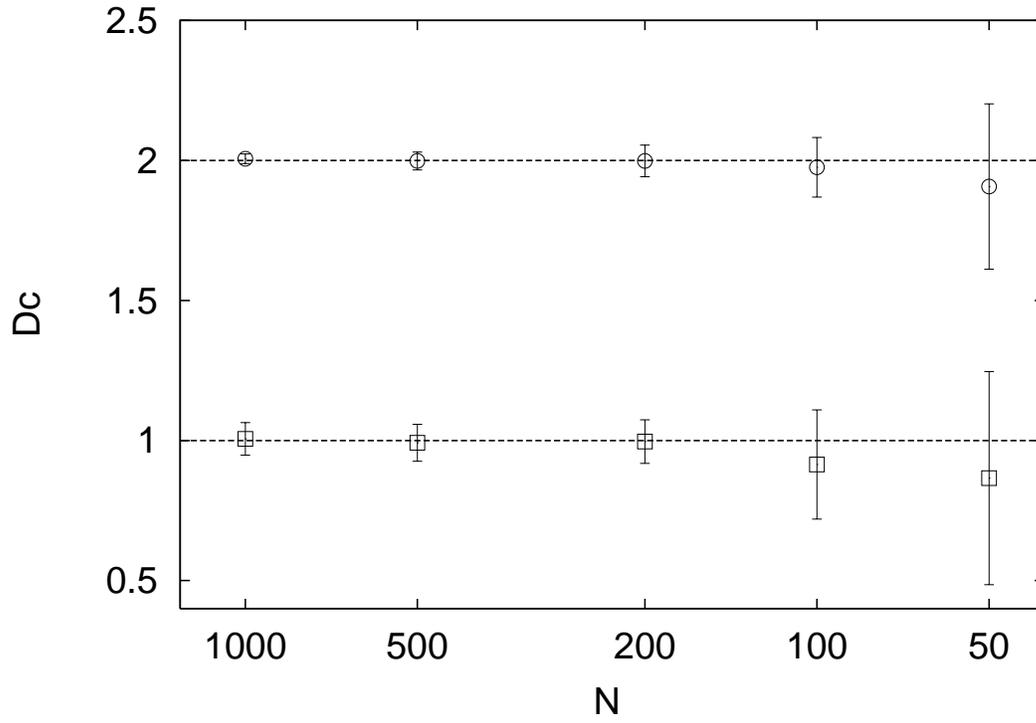


Fig. 2.— Calculated dimension D_c as a function of the sample size N for the case $f = 10^{-4}$. Open circles correspond to fractals with $D_f = 3$ and open squares to fractals with $D_f = 2$. Each point is the average of 50 random realizations and the bars show the standard deviations. Dashed horizontal lines show the expected results for thin slices.

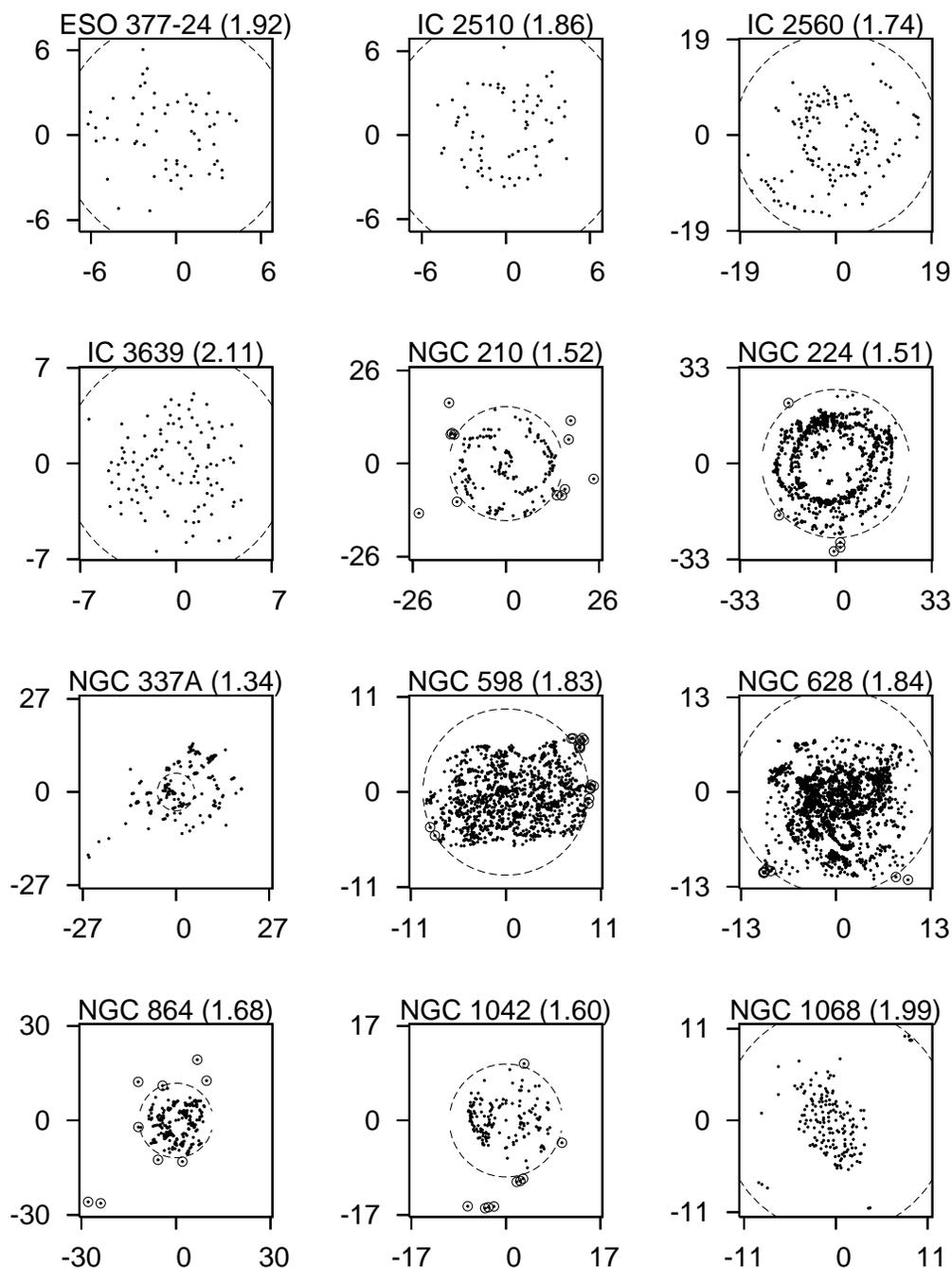


Fig. 3.— Positions of the HII regions in the galaxy sample according to references given in Table 2. The numbers in parenthesis are the corresponding fractal dimensions (Table 3). The axis units are kpc. Dashed line circles indicate the radius R_{25} . Points surrounded by circles are not taken into account when calculating D_c (see text).

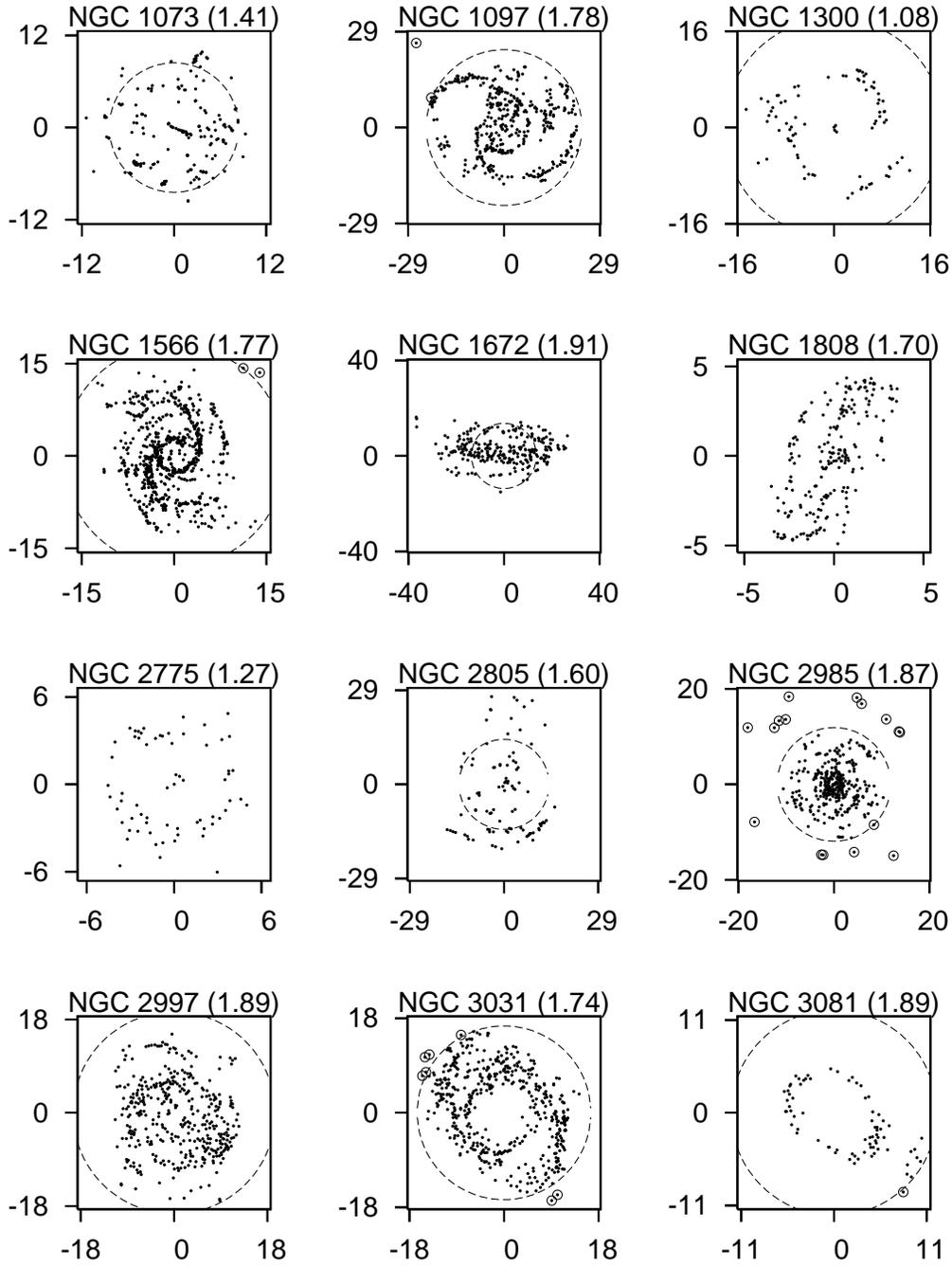


Fig. 3. — Continued.

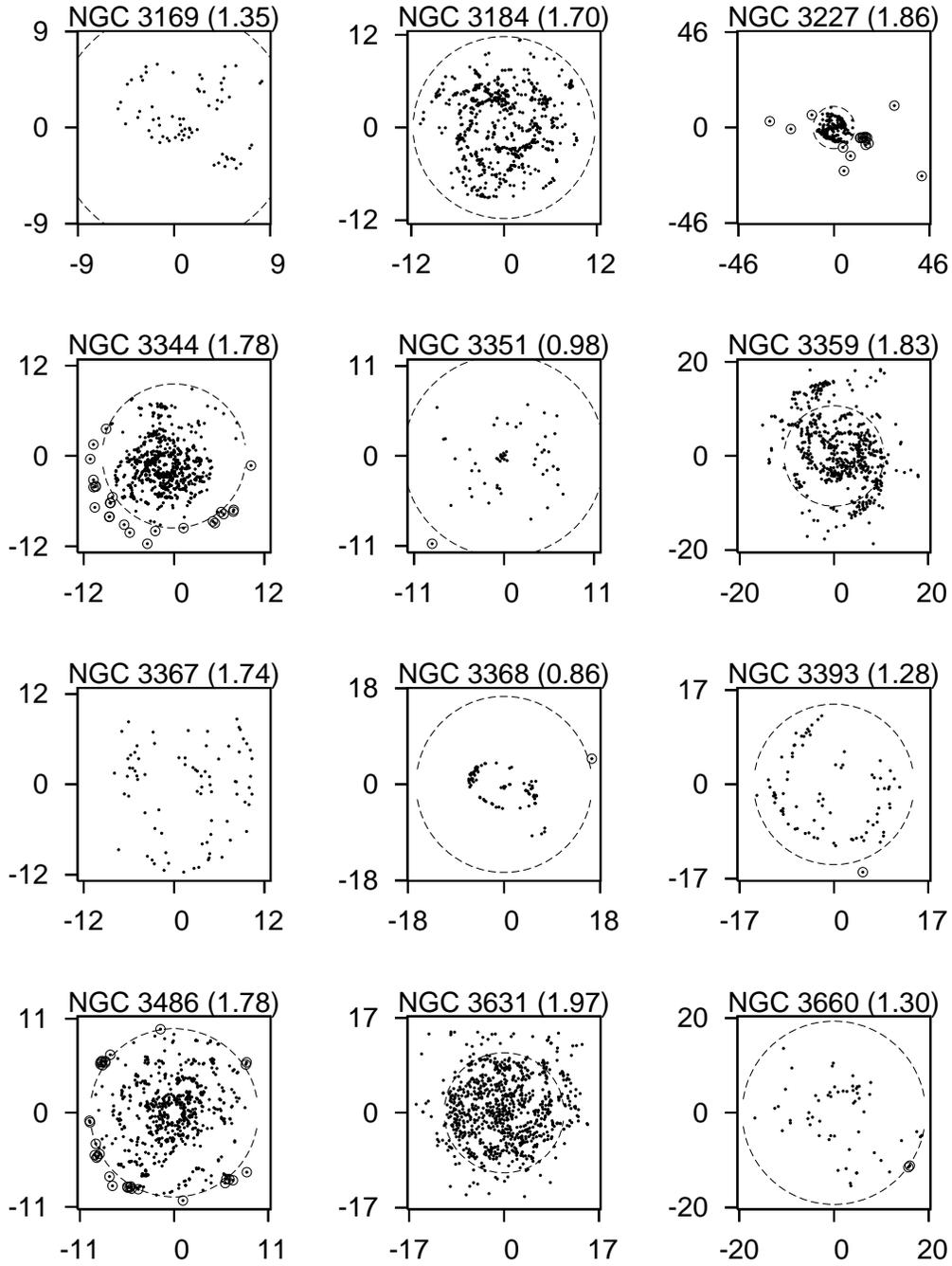


Fig. 3. — Continued.

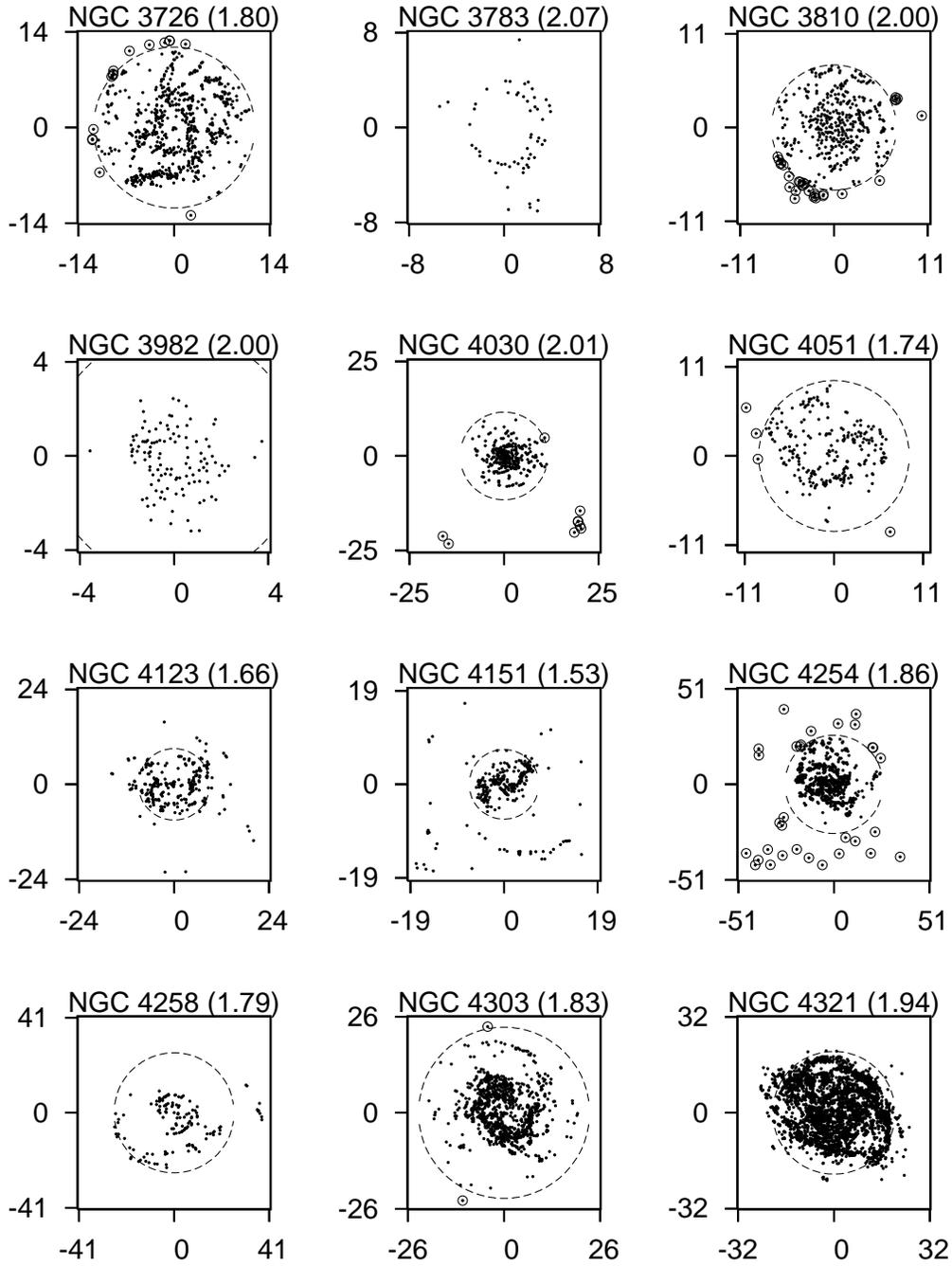


Fig. 3. — Continued.

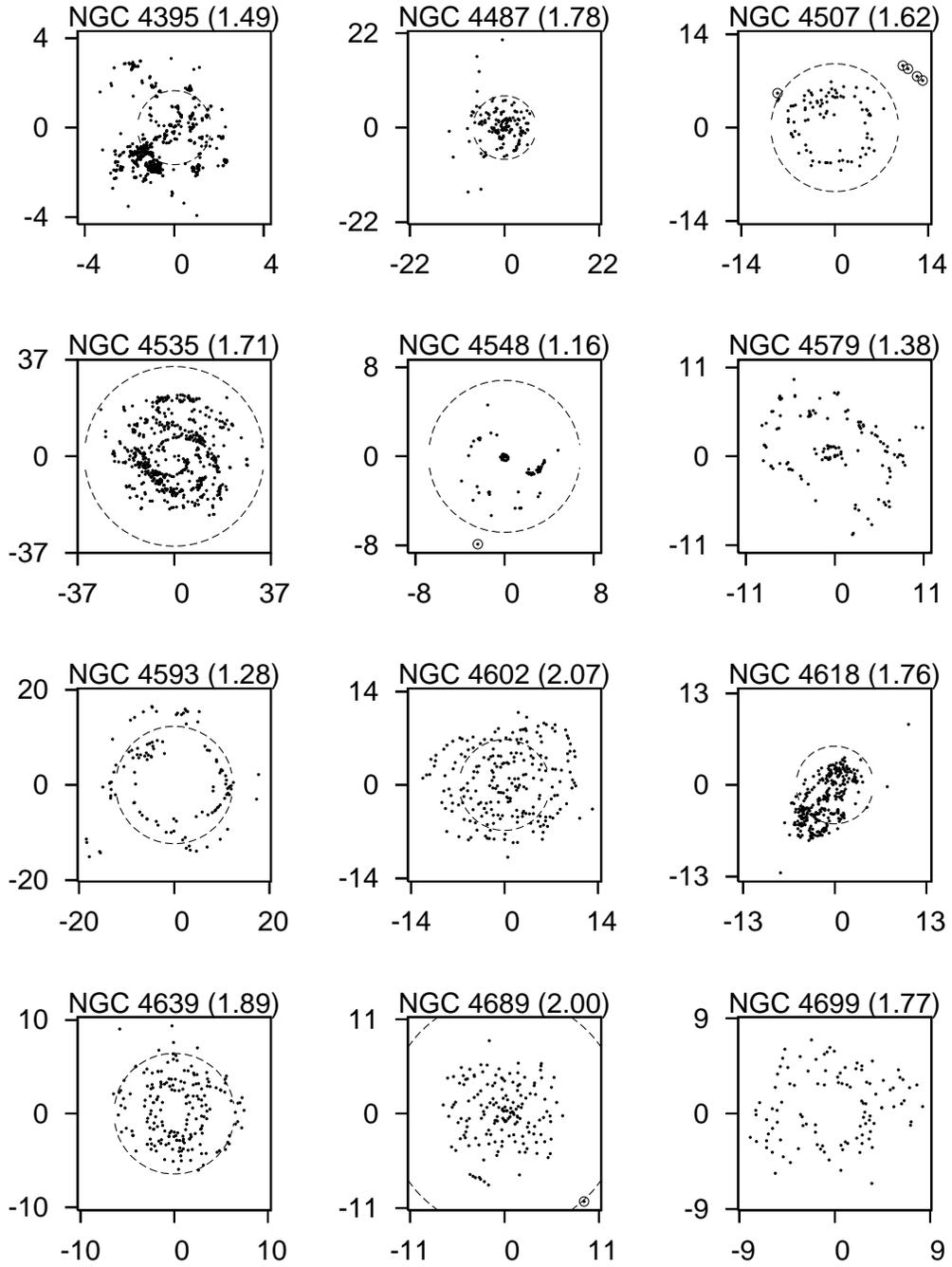


Fig. 3. — Continued.

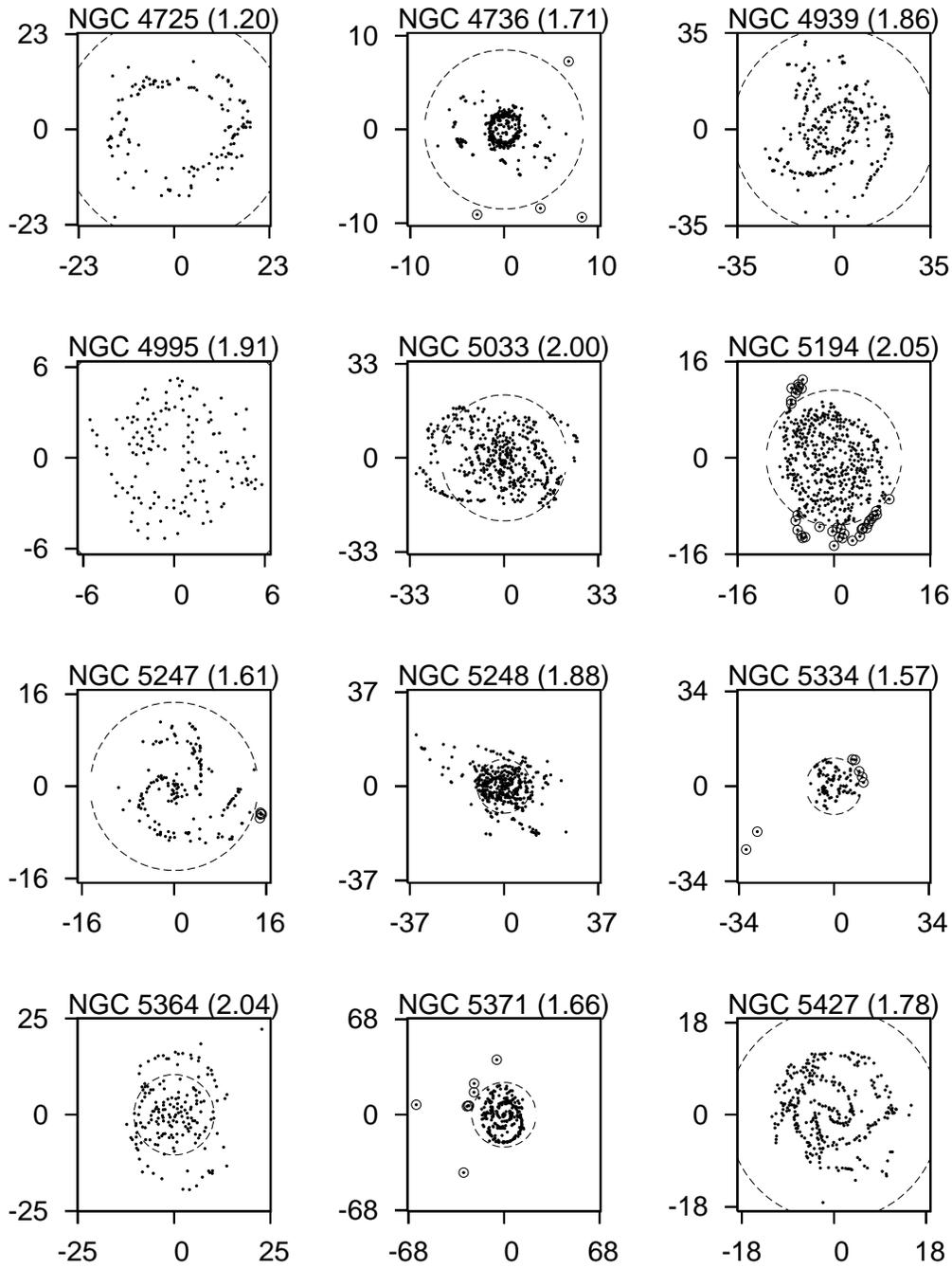


Fig. 3. — Continued.

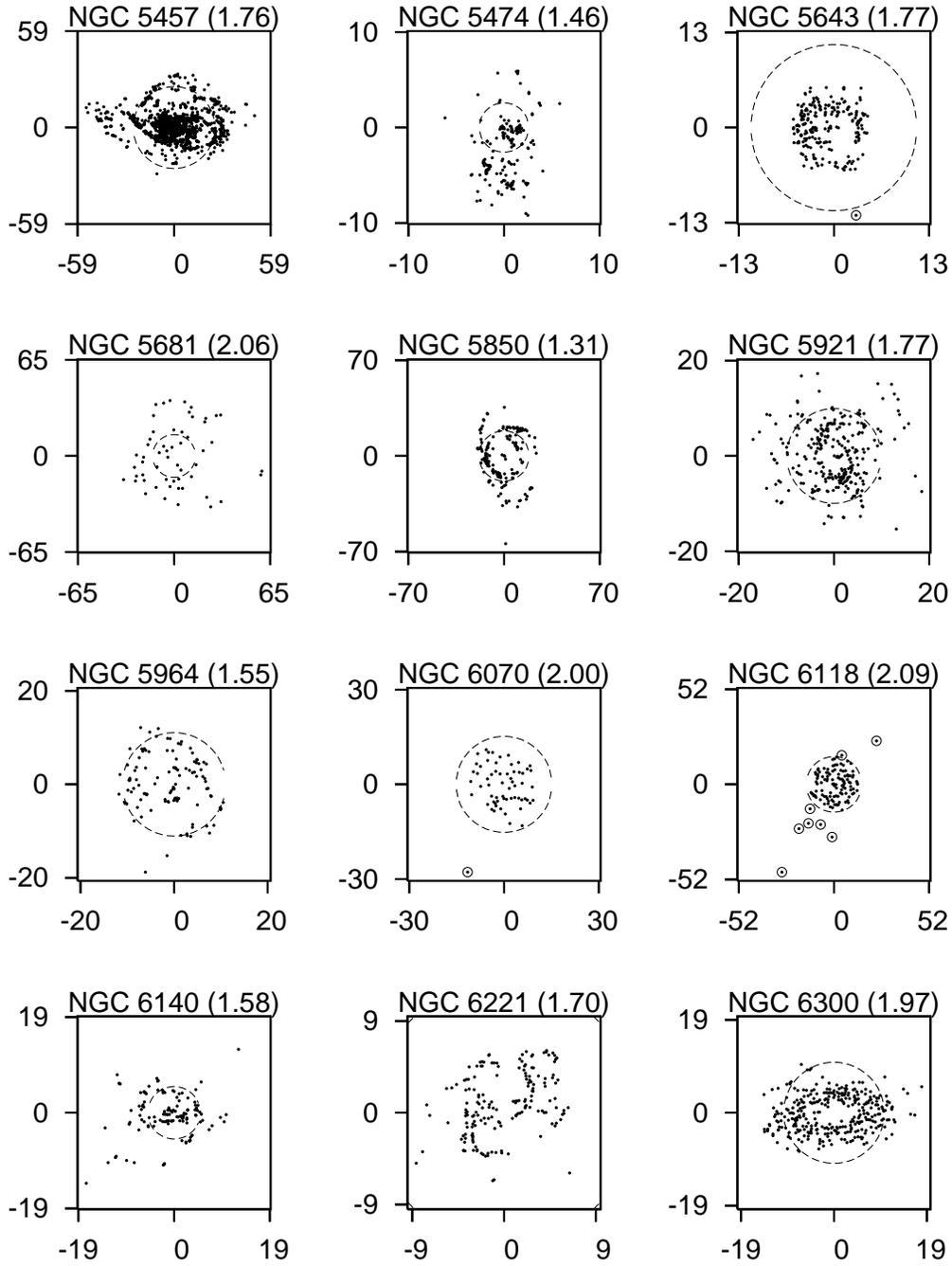


Fig. 3. — Continued.

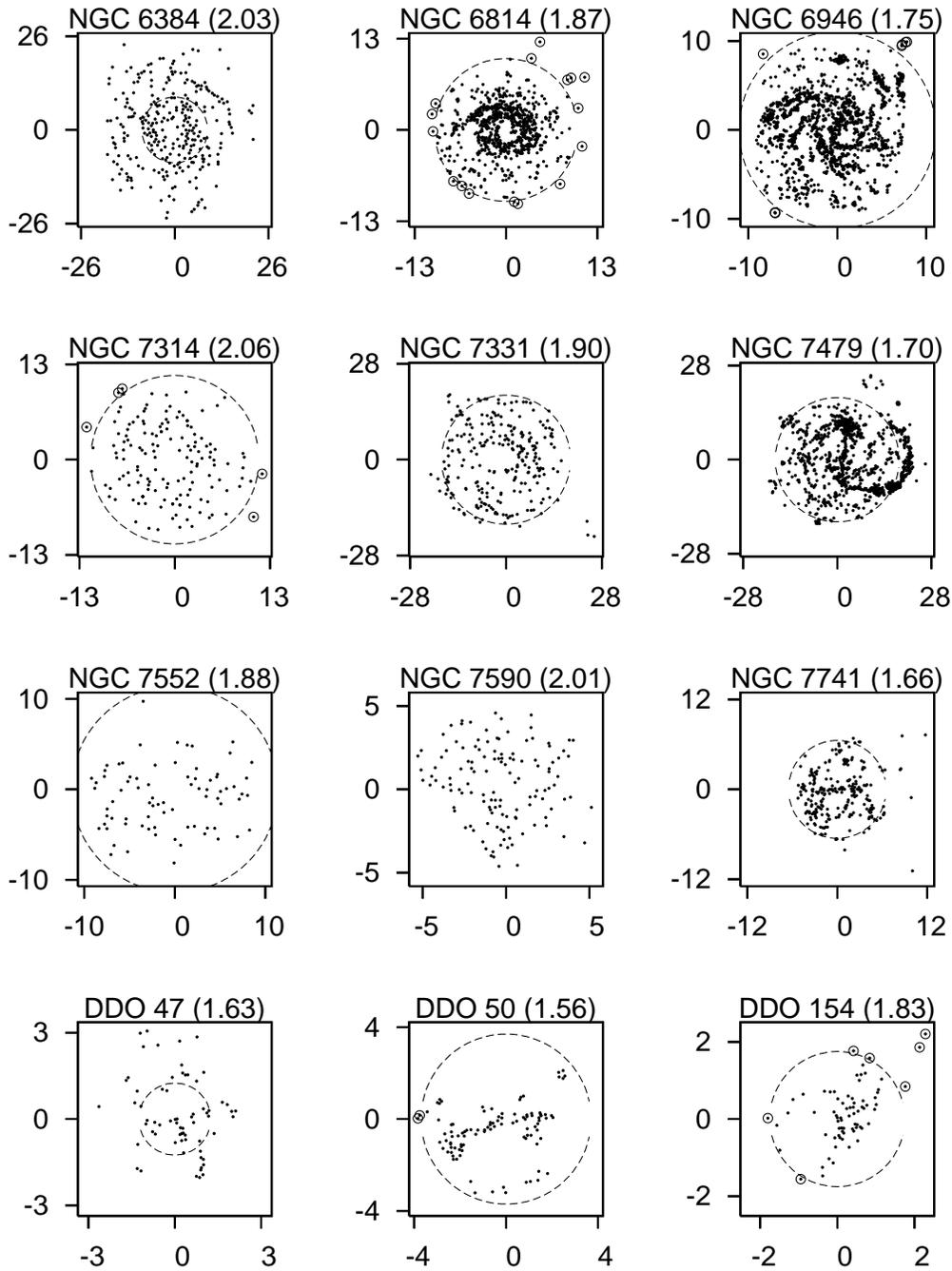


Fig. 3. — Continued.

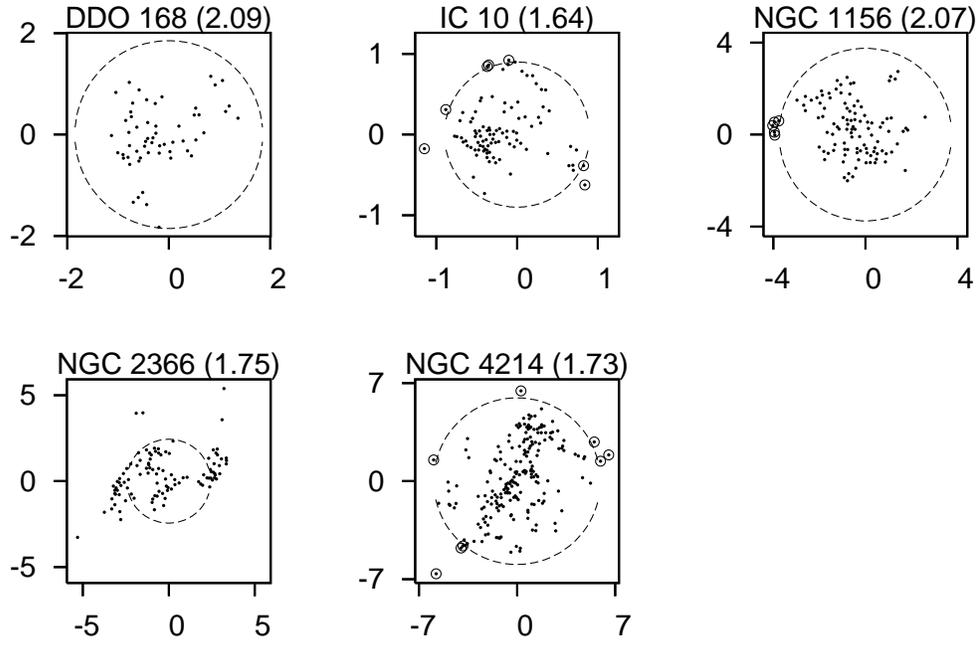


Fig. 3. — Continued.

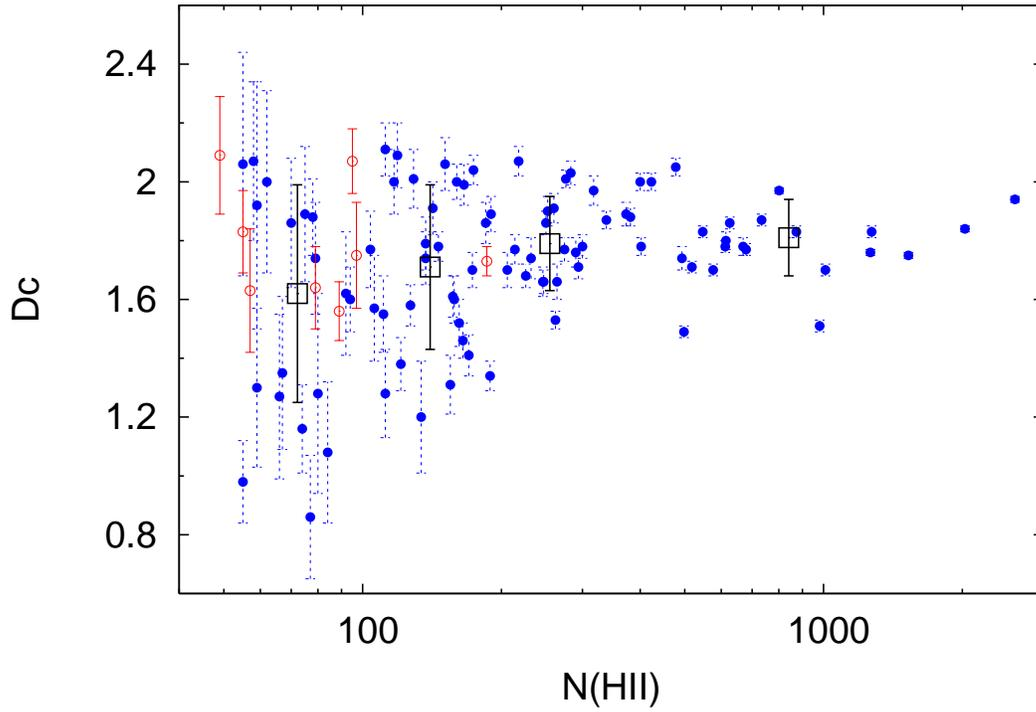


Fig. 4.— Calculated dimension D_c as a function of the number of available data $N(\text{HII})$ for spiral galaxies (blue solid circles) and irregular galaxies (red open circles) in the sample. The error bars indicate the uncertainties obtained from bootstrapping. Superposed (black squares) are the mean D_c values with their standard deviations as a function of the mean number of HII regions for four bins having the same number of galaxies (Table 4).

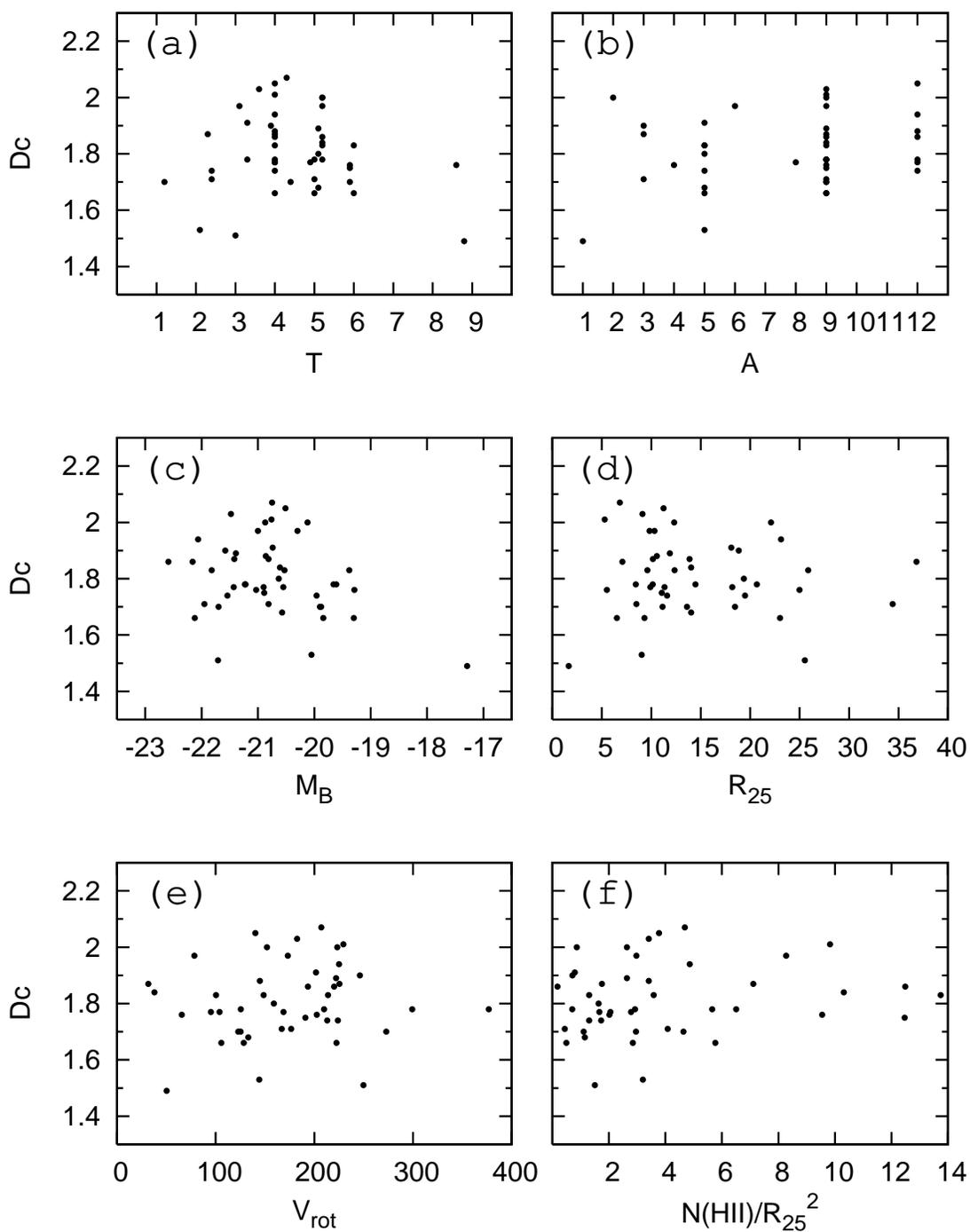


Fig. 5.— Calculated dimension D_c as a function of (a) morphological type T , (b) arm class A , (c) absolute magnitude M_B , (d) radius R_{25} , (e) rotation velocity V_{rot} , and (f) average surface density of star forming regions $N(\text{HII})/R_{25}^2$. Only galaxies having $N(\text{HII}) > 200$ have been plotted.

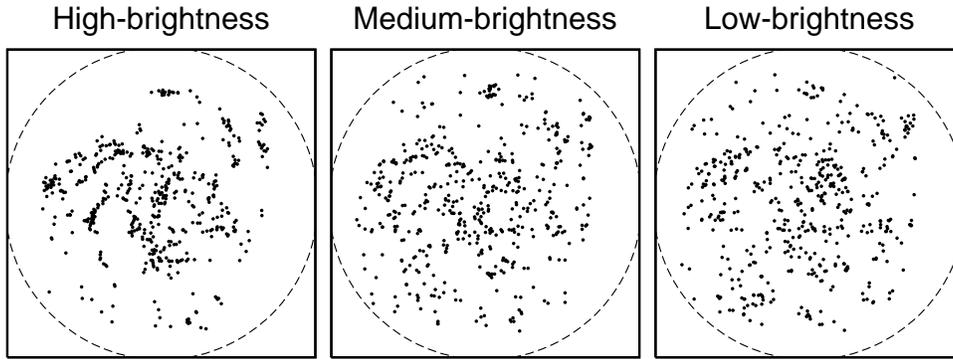


Fig. 6.— Positions of the HII regions in the galaxy NGC 6946 for high, medium, and low brightness regions (see text). The resulting fractal dimensions were $D_c = 1.64$ (high-brightness), $D_c = 1.82$ (medium-brightness), and $D_c = 1.79$ (low-brightness).